Electronic Communication through Unsaturated Hydrocarbon Bridges in Homobimetallic Organometallic Complexes

Paulina Aguirre-Etcheverry and Dermot O'Hare*

Chemistry Research Laboratory, Department of Chemistry, University of Oxford, Mansfield Road, Oxford, OX1 3TA

Received November 23, 2009

Contents

1. Introduction and Scope of Review 4839
2. Theoretical Aspects 4840
   2.1. Mixed-Valence Systems 4840
   2.2. Electron-Transfer Theory 4840
   2.3. Electrochemistry 4842
   2.4. EPR and ^{57}Fe-Mössbauer Spectroscopy 4843
   2.5. NMR Spectroscopy and X-ray Crystallography 4843
   2.6. Theoretical Calculations 4844
   2.7. IR Spectroscopy 4844
   2.8. Classification and General Properties 4844
3. Systems with Unsaturated Carbon Chain Bridges 4844
   3.1. All-Carbon sp-Bridged Systems 4845
   3.2. Carbon-Based sp^2-Bridged Systems 4848
   3.3. Carbon-Based sp/sp^2-Bridged Systems 4851
4. Systems with Aromatic Rings as Bridges 4856
   4.1. Fulvalene and Fulvalene-like Bridged Systems 4856
   4.2. Fused Delocalized Polycyclic Bridged Systems 4857
      4.2.1. Indene, Pentalene, Permethylpentalene, and Naphthalene 4858
      4.2.2. *s*-Indacene, *as*-Indacene, and Permethylfluorene 4860
5. Summary 4861
6. Acknowledgments 4862
7. References 4862

1. Introduction and Scope of Review

Bimetallic (binuclear metal) complexes contain two metal centers, either linked directly or, as in the complexes considered in this review, through a bridging ligand. Homometallic complexes may have equivalent and nonequivalent metal centers, respectively. An interesting characteristic of these compounds is the possibility for metal−metal interactions, also referred to as having a cooperative effect, depending on the nature of the ligands. A result of this effect is that the physical and chemical properties of one of the metal centers can vary substantially because of the vicinity of the other.[1–7]

There has been great interest in recent years in the study of molecules in which two metal centers show a pronounced electronic interaction across the bridging ligand. Applications may be found in molecular electronics and as models for electron-transfer processes in biological processes.[7–19] These complexes can also display enhanced or unique reactivity in stoichiometric and catalytic reactions.[20,21]

Bimetallic complexes are often precursors of stable mixed-valence species because of a strong electronic interaction across the bridging ligand. In these systems, the stability is possible as the two metal centers exist in different oxidation states, generated chemically or electrochemically. The magnetic, optical, and redox properties of these type of complexes depend on the strength of the electronic interactions between the metal centers.[22,23]

To promote the cooperative effect between the metal centers, the bridging ligand should be able to provide an electronic coupling pathway. As the degree of communication is primarily controlled by the ligand, the success on metal−metal interactions in a bimetallic complex is dependent on key ligand properties, such as flexibility and the degree of delocalization, which depends on the potential for effective orbital overlap between frontier orbitals associated with the metal and bridge fragments. For example, conjugated systems should be able to mediate the electronic interactions through their π-orbitals. It is also possible to change the metals and ancillary ligands bound to the bridging ligand or the metal oxidation state to induce significant chemical and physical properties to the systems.[8,19–21] These changes will permit further understanding and comparisons of different complexes with identical bridging ligands.

Paulina Aguirre-Etcheverry was born in Santiago, Chile, in 1979. She received her B.Sc. and a Professional Title in Industrial Chemistry in 2003 from Pontificia Universidad Católica de Chile, having done undergraduate research in Prof. J. M. Manríquez's group on the organometallic chemistry of *s*-indacene. She received her D.Phil. in chemistry from the University of Oxford in 2008, under the supervision of Prof. D. O'Hare, investigating metal−metal interactions in bimetallic organometallic complexes. She is now engaged in postdoctoral work in coordination chemistry with Prof. A. Williams at the University of Geneva.

* To whom correspondence should be addressed. E-mail: dermot.ohare@chem.ox.ac.uk. Tel: +44 (0) 1865 272686. Fax: +44 (0) 1865 285131.

10.1021/cr9003852
Published on Web 04/19/2010

Dermot O'Hare was born in Newry, Co Down and studied at Oxford University were he obtained a BA in 1982 and his D.Phil in 1985 under the direction of Professor MLH Green. In 1985, he was awarded a Royal Commission of 1851 Research Fellowship, and after a postdoctoral stint with Professor J. S. Miller at E. I. Dupont in Wilmington, Delaware, he returned to Oxford as a University lecturer and a Septcentenary Tutorial Fellowship at Balliol College. He was honoured by the Institût de France, Académie des Sciences in 1996 as one of the top 50 leading scientists in Europe under 40 yrs. He was the Royal Society of Chemistry Sir Edward Frankland Fellow in 1996, and in 1997, he received the Exxon European Chemical and Engineering Prize. In 1998, he was awarded the Royal Society Chemistry Corday Morgan Medal and Prize for his work on the structure and kinetics of intercalation of organometallic compounds in layered materials. In 1998, he became Professor of Chemistry. His scientific interests are wide ranging, and include exploratory synthetic organometallic chemistry, intercalation chemistry, time-resolved, in situ diffraction studies, and the synthesis of meso- and microporous solids.

This review will focus mainly on synthesized homobinuclear transition metal complexes (and heterobinuclear, where necessary and for comparison only) containing unsaturated hydrocarbon bridges. Ceccon et al.[20] has produced an excellent overview of homo- and heterobimetallic systems published before 2004, so our emphasis is on those systems in which metal−metal interactions have been studied post 2004. With a few exceptions, these complexes do not present metal−metal bonds. Polymeric and ligand systems containing nitrogen, sulfur or other heteroatoms as the main binding site for the metal center have not been considered.

The complexes reviewed can be classified in two general groups, depending on the nature of the unsaturated hydrocarbon bridge: (a) bridging unsaturated carbon chains containing sp- and/or sp^2-bridges, where the metal is σ-bonded to the C atom, and (b) bridging aromatic rings linked directly (fulvalene), separated by hydrocarbon chains or fused aromatic bridges; having π-coordinated metal centers.

2. Theoretical Aspects

Intramolecular electron-transfer represents one of the major topics in organometallic research.[11,24,25] Much of the interest in the study of binuclear complexes lies in the aspects that regulate the intramolecular electronic communication between the two metal centers. These are the metal-to-metal distances, the extent of conjugation in the bridging ligands, and the nature of the ancillary ligands.

2.1. Mixed-Valence Systems

Most of the techniques used to study metal−metal interactions are applied to mixed-valence species, which are among the simplest model systems for studying electron-transfer and

Scheme 1. Formation of Mixed-Valence Compounds (Class I and Class II) M_1^{n+1}-L-M_2^{n} and M_1^{n}-L-M_2^{n+1} (K_c = Comproportionation Constant)

$$M_1^{n}-L-M_2^{n} + M_1^{n+1}-L-M_2^{n+1} \overset{K_c}{\rightleftharpoons} M_1^{n+1}-L-M_2^{n} + M_1^{n}-L-M_2^{n+1}$$

mixed-valence systems

Scheme 2. Totally Delocalized Class III System with a Large K_c

$$M_1^{n}-L-M_2^{n} + M_1^{(n+1)}-L-M_2^{(n+1)} \overset{K_c}{\rightleftharpoons} 2\,M_1^{(n+1)/2}-L-M_2^{(n+1)/2}$$

delocalization.[26,27] As mentioned before, these complexes present two (redox-active) metal centers (M_1 and M_2), one in oxidation state n and the other in oxidation state ($n + 1$), linked by a bridging ligand L. As a consequence, the sites are not equivalent and there exists a barrier to their interconversion.

The equilibrium displayed in Schemes 1 and 2 represents the formation of mixed-valence systems. K_c is the comproportionation constant that represents the relative stability of these species (section 2.3). Large values of K_c are essential for the isolability of the mixed-valence compounds.[28] Strongly delocalized systems often present large K_c values; however, this cannot be used as a direct measurement of the delocalization of mixed-valence complexes,[17,24–29] as discussed in more detail in section 2.3.

The strength of the electronic interactions between M_1 and M_2 varies from zero or weak (class I) to moderate (class II) and to very strong (class III) according to the classification of mixed-valence species proposed by Robin and Day.[29]

Class I complexes present optical and electronic properties for the separate sites M_1^{n} and M_2^{n+1} or M_1^{n+1} and M_2^{n}. Activated electron-transfer either does not occur at all or only at a very slow rate. Class II systems display new optical and electronic properties in addition to those of the separate sites. However, the interaction is weak therefore the systems are valence trapped or charge localized. In class III species, the electronic coupling is very strong, the odd electron is fully delocalized and the systems show unique electronic and optical properties. Detailed descriptions and criteria for classes are given in the following section.

2.2. Electron-Transfer Theory

The electronic communication within a system can be regarded in terms of the electron-transfer theory introduced by Marcus,[30–33] which aims to explain the transfer of electrons between two metal centers. Figure 1 represents a binuclear metal complex where the two metals correspond to the donor and the acceptor sites. They are connected by a bridging ligand. The donor and acceptor represent the places between which the electron-transfer occurs.

If a symmetrical bridging ligand and both donor and acceptor sites only differing in their oxidation states are considered, there is a difference in the intramolecular equilibrium and the solvent configuration at the donor and

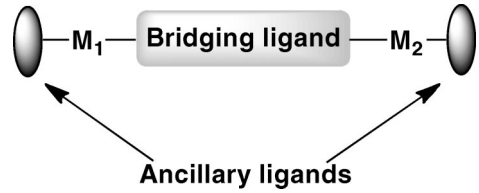

Figure 1. Representation of a bimetallic metal complex: M_1 and M_2 are linked through the bridging ligand.

the acceptor sites. Therefore both sites are not equivalent, with a barrier for their interconversion. The intramolecular electron transfer can be described in terms of the motion of the system on an energy surface from the initial state toward the activated complex and then to the final state. Thus, electron-transfer processes can be regarded as a common chemical reaction. Depending on the interplay between the nuclear and electronic frequencies, electron-transfer reactions are categorized as adiabatic or nonadiabatic. A system is considered to be weakly coupled when a nonadiabatic electron-transfer occurs and strongly coupled when an adiabatic transfer happens.[34,35]

When the electron moves from the donor to the acceptor, the nuclear configuration of the reactants and their surrounding media adjust from their equilibrium values to an intermediate configuration in which there is no energy change. This is required by the energy conservation principle, also considering that electron motion is much faster than nuclear motion. The nuclear configuration changes comprise adjustments in the metal−ligand and intraligand bond lengths and angles. It also requires changes in the orientations of the surrounding solvent molecules.

The expression of the kinetic rate constant for a generic electron-transfer process (k_{ET}) is given by transition state theory (eq 1) where k_{el} is the transmission coefficient, ν_n is the frequency of passage (nuclear motion) through the transition state, k_B is the Boltzmann constant, λ is the reorganization energy, ΔG° is the total Gibbs free energy change for the electron-transfer reaction, and T is temperature. λ has been defined as the difference in Gibbs energy if the reactant state remained unchanged at the equilibrium configuration but electron-transfer occurs.[33,34,37] $\Delta G^\#$ is the free energy of activation. From pure geometrical considerations, the following relations for $\Delta G^\#$ have been obtained. When $\Delta G^\circ = 0$, then $\Delta G^\# = \lambda/4$. If $\Delta G^\circ \neq 0$, then $\Delta G^\# = (\lambda + \Delta G^\circ)^2/4\lambda$.[20]

$$k_{ET} = k_{el}\nu_n \exp\left[-\frac{(\lambda + \Delta G^\circ)^2}{4\lambda k_B T}\right] \quad (1)$$

Marcus theory is widely accepted for electron-transfer processes in chemistry because it makes several predictions that have been verified over the last decades.[33,36] The most significant being that the rate of electron-transfer will increase as the electron-transfer reaction becomes more exothermic but only to a point. Past that point, the electron-transfer rate will actually decrease as the reaction becomes more exothermic, in the so-called "Marcus inverted region". Empirical proof of this has been found by several authors.[37–54]

This theory was then extended to inner sphere electron-transfer transitions by Hush, which can be applied to stable mixed-valence systems.[55–57] These species can be studied by spectroscopic analyses that, along with cyclic voltammetry (CV) studies, often allow the determination of the type (class) of mixed-valence complex. They often present a weak intervalence charge transfer (ICT) band characteristic of the optically induced intramolecular electron-transfer, typically in the near-infrared (NIR) spectral area, which is absent in the spectra of the reduced and oxidized states.

Simple Hush theory allows the determination of the two most important electron-transfer parameters from the ICT band, the reorganization energy λ and the electronic matrix coupling H_{ab}. The latter one arises from donor and acceptor coupling.

The interplay between H_{ab} and λ in a mixed-valence complex determines the class to which the system belongs. A class I complex has a completely localized charge ($H_{ab} = 0$) and no intramolecular electron-transfer between the donor and the acceptor will occur. Experimentally, a complex might be assigned to be class I when H_{ab} is immeasurably small and no ICT band is observed. Activated electron-transfer either does not occur at all or occurs only very slowly with $\Delta G^\# = \lambda/4$. $H_{ab} < \lambda/2$ corresponds to a class II system and $\Delta G^\# = (\lambda - 2H_{ab})^2/4\lambda$, as long as the system remains valence trapped. When $H_{ab} \geq \lambda/2$, the complex is completely delocalized and corresponds to a class III species, having a $\Delta G^\# = 0$.

In symmetric homobimetallic class II mixed-valence species ($\Delta G^\# = (\lambda - 2H_{ab})^2/4\lambda$), the expression of the kinetic rate constant can be expressed in terms of H_{ab}, leading to eq 2. The prefactor A is dependent on the electronic coupling. In relatively weakly coupled systems (nonadiabatic electron-transfer), the motion of the electron is slower than that of the nuclei and A is a function of H_{ab} and λ. However, in strongly coupled systems (adiabatic electron-transfer), the limiting factor is the motion of the nuclei.[34,58,59]

$$k_{ET} = A \exp\left[-\frac{\lambda - 2H_{ab}}{4\lambda k_B T}\right] = k_{el}\nu_n \exp\left[-\frac{\Delta G^\#}{k_B T}\right] \quad (2)$$

Class II species are characterized by a value of H_{ab} sufficiently large to result in an experimentally observable ICT band. In these species, $\bar{\nu}_{max} = \lambda$ and is not dependent upon H_{ab}, but is often strongly dependent upon the solvent (due to the solvent contribution to the external reorganization energy, which arises due to the large dipole moment change associated with the ICT). H_{ab} (cm^{-1}) for class II systems can, however, be extracted from the ICT band using Hush's formalism, with a general and fundamental expression (eq 3). In this expression, μ_{ge} is the transition dipole moment of the ICT band, R is the effective separation between donor and acceptor in the case of nonadiabatic states and e is the electronic charge.

$$H_{ab} = \frac{\mu_{ge}}{eR}\bar{\nu}_{max} \quad (3)$$

In the case of symmetric Gaussian-shaped ICT bands, eq 4 can be used. In this expression, $\Delta\bar{\nu}_{1/2}$ is the bandwidth at half height for a Gaussian-shaped ICT band (cm^{-1}), ε_{max} is the extinction coefficient at the band maximum ($M^{-1}cm^{-1}$), and R is the effective separation between the donor and acceptor sites in the case of nonadiabatic states in angstrom.[60,61]

$$H_{ab} = \left(\frac{0.0206}{R}\right)(\bar{\nu}_{max}\Delta\bar{\nu}_{1/2}\varepsilon_{max})^{1/2} \quad (4)$$

A problem of using eq 4 is in defining the appropriate value of the nonadiabatic electron-transfer distance R. In other words, R is the distance between the centers of the two redox sites in the absence of electronic coupling. This assumption is often true for weakly coupled species. However, any delocalization of the charge will lead to reduced values of R. This is because the bridge orbitals make a significant contribution to the nonadiabatic states, leading to smaller values of R than the geometric distance and H_{ab} will be underestimated.[43,46–48]

In symmetrical class III systems, the odd electron is delocalized between the metal centers and the energy of the optical transition is given by $h\bar{\nu}_{max} = 2H_{ab}$. Therefore H_{ab} can be calculated directly from this transition.[34]

For symmetrical species ($\Delta G^\circ = 0$), Hush theory predicts that the bandwidth at half height is given by eq 6, which at room temperature, reduces to eq 5.[34]

$$\Delta\bar{\nu}_{1/2}(cm^{-1}) = (2310\bar{\nu}_{max})^{1/2} \quad (5)$$

$$\Delta\bar{\nu}_{1/2} = (16RT \ln 2\lambda)^{1/2} \quad (6)$$

Comparison between the calculated and observed $\Delta\bar{\nu}_{1/2}$ may be useful to classify a complex, as class III systems typically exhibit ICT bands with widths narrower than the Hush limits given in eqs 5 and 6, while the bands of class II species are typically broader than the theoretical limit. Class III systems also display higher peak intensities (ε) and only weak solvent dependence.[62] In fact, eqs 5 and 6 do not apply to class III systems.

Mixed-valence complexes possessing transition metal centers corresponding to class II may lie nearer to the borderline II/III and present very fast thermal electron-transfer. These systems can be defined by introducing the mixing coefficient α, approximated to $H_{ab}/\bar{\nu}_{max}$. This coefficient is related to the degree of mixing between the two limiting localized initial and final electronic states. However, this approximation becomes more invalid as the borderline is approached. Equation 7 shows a method by which a system can be classified, using the delocalization parameter Γ.[34] It is a useful tool, along with H_{ab}, to determine whether a complex is weakly, moderate or strongly coupled. Weakly coupled class II systems display values of $0 < \Gamma < 0.1$; moderately coupled class II, $0.1 < \Gamma < 0.5$; borderline class II/class III, $\Gamma \approx 0.5$; and class III, $\Gamma \gg 0.5$. It is important to notice that Γ is based on the width of the ICT band. We assume that this method is more conclusive for the complexes presented in this review.

Meyer et al.[63] have extensively reviewed these class II/class III systems, focusing in the transition from localized to delocalized mixed-valence complexes. These species present intermediate properties between class II and class III. They have been described as "almost delocalized" mixed-valence complexes. The features that characterize these class II/class III systems are: electronic localization, solvent averaging (electron-transfer is too fast and the solvent cannot keep up with the motion of the transferring electron) and a residual barrier to electron-transfer arising from intramolecular structural changes.

$$\Gamma = \left[1 - \frac{\Delta\bar{\nu}_{1/2}}{(2310\Delta\bar{\nu}_{max})^{1/2}}\right] \quad (7)$$

Kubiac et al.[64] have studied the solvent effects in complexes that correspond to the borderline class II/class III systems by IR spectral analysis. They concluded that, in the nearly delocalized limit, solvent thermodynamic parameters do not significantly influence rates of electron transfer (solvent reorganization energy, solvent polarity, and static dielectric constants). However, solvent relaxation can limit the rate of the electron-transfer in the type of systems studied.

Although the Hush theory is the preferred method for analyzing mixed-valence complexes, it is only applicable to weakly interacting systems. Difficulties occur when applying this theory to more strongly interacting species.[65,66] Indeed, in delocalized systems (class III), the ICT band can no longer be considered as the transfer from one metal center to the other because the electron is shared equally between the two. Therefore, the transfer of an electron from one delocalized orbital to another represents the transition.[67] Hush equations to calculate H_{ab} may be valid if R is properly assigned.[68] The classical Hush treatment has been successfully applied to understand the electron-transfer in symmetrical purely inorganic mixed-valence systems. However, this model has been rarely used to study unsymmetrical systems.[69]

Piepho, Krauz, and Schatz developed a vibronic coupling model (PKS model) to calculate absorption profiles applicable to class II and class III systems.[70] Creutz, Newton, and Sutin introduced a new optical method (CNS model) to determine H_{ab} by analyzing the often higher energy, and easier to recognize, metal to ligand charge transfer band (MLCT) in UV−vis spectroscopy. This model has been applied to binuclear mixed-valence ruthenium complexes displaying valence trapped to nearly delocalized behavior.[71,72]

Experimental studies of the ICT bands in mixed-valence complexes have provided important insights into the fundamental intra- and intermolecular factors that govern electronic delocalization and the activation barrier to electron-transfer. These arise from environmental contributions such as ion-pairing, solvation, temperature of the medium and intramolecular contributions due to structural factors. The latter are dependent on the identity and coordination environments of the metal centers. Also, significant stereochemical effect on the ICT band have been attributed to environmental contributions such as inherent structural distortions in the bridging ligand, specific solvation effects and stereochemically directed anion and solvent interactions. In general, complexes incorporating nonrigid bridging ligands present an additional complexity as the inherent structural distortion induces an effective redox asymmetry contribution. In the case of diastereoisomers presenting rigid bridging ligands, the most important factors contributing to the ICT band are anion and solvent interactions as well as the temperature of the medium.[7,57,63,73–81] For a detailed description of intra- and intermolecular contributions to the ICT band, the reader is invited to refer to the reviews by D'Alessandro and Keene.[75,81]

2.3. Electrochemistry

The easiest way to look at the electronic interactions between two active sites of a molecule is by using an electrochemistry technique called cyclic voltammetry (CV). In a complex containing two metal centers and in the case of a strong interaction, two electrochemistry events should be observed. The potential difference (ΔE) between the two reversible waves (E_1 and E_2) is representative of the thermodynamic stability of the corresponding mixed-valence state relative to the other redox states ($\Delta E = E_2 - E_1$).[13,15,17] ΔE is generally proportional to the thermodynamic stability of the mixed-valence complex (under the conditions of solvent and electrolyte used). Therefore, it is useful for evaluating the possibility for isolating the mixed-valence species.

In symmetrical homobimetallic complexes, where $M_1 = M_2$, ΔE is an indicator of the interactions between the two metal centers (assuming that both waves are reversible) but is a not a direct measurement of the electronic coupling H_{ab}, and it cannot be used to conclusively determine to which

class a system belongs. If the values of ΔE are close to zero, the metals are noninteracting either because of the great distance between them or because the ligand does not provide an electronic coupling pathway. Usually these systems belong to class I. A small ΔE separation represents a weak interaction between the metals with a small value for the comproportionation constant, $K_c = e^{\Delta EF/(RT)}$ for the equilibrium represented in Scheme 1 (F = Faraday constant = 96485.33 C/mol). This situation is commonly assigned to a mixed-valence state involving trapped-valence systems (class II). A larger value of ΔE corresponds to a totally delocalized system with a very large K_c (Scheme 2), and there is a stabilization of the mixed-valence species, normally assigned to class III.[20] The redox centers are so strongly coupled that the lone-electron is delocalized and only a single average valence state can be assigned to the two centers ($M_1^{(n+1)/2} = M_2^{(n+1)/2}$). However, some class III compounds may present very small ΔE values. For example, the organic compound (*E*,*E*)-1,4-[bis-{bis(4-methoxyphenyl)-amino}styryl]benzene displays a rather large coupling of $H_{ab} = 1400$ cm^{-1} and a small ΔE value of 140 mV.[68] The complex *anti*-[Mn(CO)$_3$]$_2$(μ:η^5:η^5-Pn) presents very large coupling of 6400 cm^{-1} and a ΔE values of 410 mV (Pn = pentalene-diide).[82] On the other hand, *anti*-[Cp*Co]$_2$(μ:η^5:η^5-Pn) displays a coupling of 4770 cm^{-1} and a large ΔE value of 710 mV (Cp* = pentamethylcyclopentadienyl).[83] This is contrary to what is expected as systems with large values of ΔE normally present large H_{ab} values.

Gladysz et al.[84] have pointed out the dependence of K_c on the distance between both metal centers. As the chain length increases, the value for K_c decreases. For example, the family of complexes Cp*(NO)(PPh$_3$)Re(C≡C)$_n$Re(PPh$_3$)(NO)Cp* has K_c values on the order of 10^9 for $n = 2$, 10^6 for $n = 3$, and 10^3 for $n = 5$, 6, and 8.

Therefore it is important to consider that even if a more effective conjugation along the intermetallic bridge facilitates the transfer of electronic information between metal centers, meaning a greater value of ΔE, the separation of the two redox waves can be influenced by other factors such as electrostatic interactions, solvation, ion pairing with the electrolyte and structural distortions from oxidation or reduction processes.[85–89] It is important to remember that ΔE is related to the thermodynamic stability of the mixed-valence species where other energetic terms, apart from the one related to the electronic interactions, are also considered.[13] Also, ΔE should not be used on its own to classify mixed-valence species.

For heterobimetallic complexes ($M_1 \neq M_2$), a nonzero ΔE is expected even without delocalization because of the different redox properties of metal centers present in the molecule. To study the degree of the delocalization, one has to focus on the difference between the redox potential of the reversible wave of one metal center of the bimetallic complex and the redox potential of the reversible wave of its corresponding monometallic species.[90] In general for bimetallic species, if the first redox potential is significantly lower than that of the corresponding monometallic complex, this may indicate strong coupling and delocalization.

2.4. EPR and ^{57}Fe-Mössbauer Spectroscopy

Techniques such as electron paramagnetic resonance (EPR or electron spin resonance, ESR) and ^{57}Fe-Mössbauer spectroscopy (only suitable for Fe complexes among transition metals) are appropriate to study electronic and nuclear interactions. The latter technique, which can help place a time scale on the electron exchange, has not been considered further in this review as it is only applicable to iron complexes. For an explanation and applications of ^{57}Fe-Mössbauer spectroscopy, the reader is invited to refer to *Mössbauer Spectroscopy* by Dickson and Berry.[91] The ideal situation for EPR studies occurs when the paramagnetic species have nondegenerate ground-states and hyperfine coupling can be observed. For example, bis(η-C$_6$H$_6$)vanadium possesses a $^2A_{1g}$ ground-state and ^{51}V in 99.75% abundance with nuclear spin $I = 7/2$.[63,64] Hence, electronic interactions can be studied in this system. When degenerate ground-states are analyzed, the situation is more difficult as low temperatures are often required to obtain EPR spectra. However, in some cases, hyperfine coupling can still be resolved, as in bis-(μ^2:η^5:η^5-Fv)dicobalt monocation (^{59}Co, $I = 7/2$) where a 15-line spectrum is observed (Fv = fulvalendiyl).[92,93] This indicates that the system is detrapped on the EPR time scale, that is, in this case, the system is either delocalized (class III) or is localized (class II) with an intermolecular electron-transfer rate that is large compared to the magnitude of the electron-^{59}Co coupling constant (A).

2.5. NMR Spectroscopy and X-ray Crystallography

Nuclear magnetic resonance (NMR) spectroscopy and X-ray crystallography provide useful structural information in solution and the solid state. A system presenting two metal centers in the same oxidation state is expected to generally show equivalent M−C bond distances, whereas a complex with both metal centers in different oxidation states is predicted to display two distinctive M−C bond lengths. This variation is caused by the different environments around each of the metal centers. For example, the cation [μ^2:η^5:η^5-Fv{Fe(C$_5$H$_4$I)}$_2$]$^+$[I$_3$]$^-$ features two equivalent Fe centers with average Fe−C bond distances of 2.07 Å. However, ([μ^2:η^5:η^5-Fv{Fe(C$_5$H$_4$Cl)}$_2$])$_2^+$[I$_8$]$^{2-}$ possesses two different Fe centers with average bond lengths of 2.08 and 2.03 Å.[94] Still, it might be difficult to distinguish between apparent equivalence arising from delocalization and those from static or dynamic disorder. On the other hand, an asymmetric crystal environment may lead to a localization of the cation structure that is not necessarily found in solution.

NMR spectroscopy is a useful technique when the system studied is diamagnetic. However, most of mixed-valence bimetallic organometallic complexes are paramagnetic. They display typically broad peaks from which is difficult to extract information. However, a NMR signal for V^V for example, can be detectable when the unpaired electrons are on atoms in close proximity. The interactions between these atoms and the unpaired electrons results in a broadening of the spectral lines because of electron−nuclear dipolar coupling. Solid-state NMR spectroscopy of these types of systems has been previously used to study local environment in a few inorganic systems.[95–100] The magnitude of the electron−nuclear dipolar coupling establishes whether a NMR signal is observed. This is determined by the magnitude of the electronic magnetic coupling and the distance to the paramagnetic center. This technique has been recently utilized by Lobo et al.[101] to identify mixed-valence vanadium-substituted titanosilicate complexes containing V^{IV} and V^V centers.

Scheme 3. Summary of the Properties for Each Class of Mixed-Valence Species

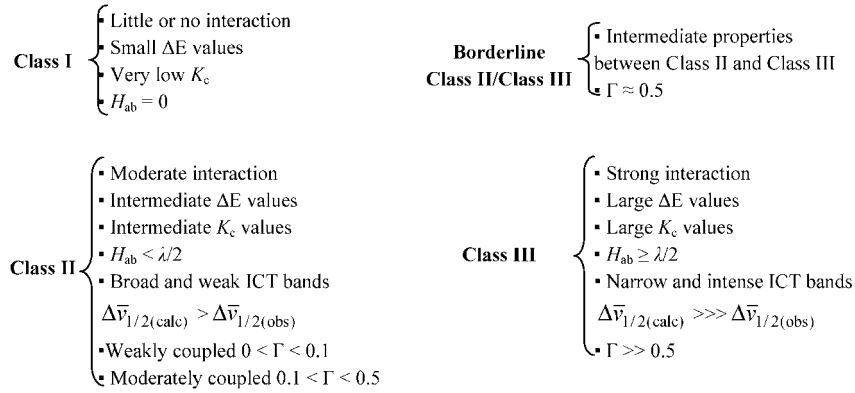

2.6. Theoretical Calculations

Theoretical calculations are also being increasingly used to understand the electron-transfer at the molecular level and to compare experimental with theoretical data. They are able to provide a fairly accurate description of the ground- and excited-states. Several studies have been developed recently to gain a better understanding of mixed-valence complexes and their properties.[102–106] However, DFT tends to overdelocalize the unpaired electron. For example, DFT could predict a class III species but experimental data suggest a class II system.[35]

2.7. IR Spectroscopy

Infrared (IR) spectroscopy is also a useful technique in distinguishing between localized and delocalized mixed-valence systems and, in some cases, to establish the rates of intramolecular electron-transfer in class II systems. Two slightly different applications of IR spectroscopy can be established. First, the IR activity of a mode of the bridging ligand in the mixed-valence state, which is IR-inactive in the fully oxidized and reduced states, indicates a breaking of the symmetry in the mixed-valence species down to the time scale of a single vibration (e.g., on the time scale of $\sim 6 \times 10^{13}$ s^{-1} for a C≡C stretching), that is, indicating that the cation belongs to classes I or II. On the other hand, in class III systems, modes of this type are expected to be IR-inactive. For example, the mixed-valence complex $[(bpy)_2(Cl)Os(pz)Os(Cl)(bpy)_2]^{3+}$ (borderline class II/class III, where bpy = bipyridine and pz = pyrazine) displays an IR-active mode for the pz group, whereas for $[(bpy)_2(Cl)Os(pz)Os(Cl)(bpy)_2]^{2+}$ and $[(bpy)_2(Cl)Os(pz)Os(Cl)(bpy)_2]^{4+}$, these modes are IR-inactive.[59] The spectrum of IR-localized species present bands characteristic of both oxidation states of the redox units, whereas IR-delocalized systems show only new bands corresponding to the averaged mixed-valence unit. For example, ferrocene-based and ferrocenium-based complexes exhibit bands (C−H bending) at 815 and 851 cm^{-1}, respectively. The IR spectrum for the localized system $[\mu^2:\eta^5:\eta^5\text{-Fv}\{Fe(C_5H_4I)\}_2]^+$ has bands at 822 and 849 cm^{-1}, while that of the delocalized complex $\{[2.2]$ferrocenophane-1,13-diyne$\}^+$ presents a single band at 830 cm^{-1} (ferrocenophane = $CpFe(C_5H_4)(C{\equiv}C)_2(C_5H_4)FeCp$ and Cp = cyclopentadienyl).[92,94] Thus, the rates of intramolecular electron-transfer are respectively small and large compared to the differences in frequency ($\sim 1 \times 10^{12}$ s^{-1}). In some cases, the temperature dependence of IR bands that act as redox state markers (typically the stretches of CO groups) have been used to determine the rates of electron-transfer at multiple temperatures and, hence, to provide estimates for the barrier to electron-transfer (ΔG^*).[107]

2.8. Classification and General Properties

Scheme 3 summarizes the general characteristic properties for the classification of mixed-valence systems. In general, ΔE values and the ICT band in the NIR region are widely used techniques to classify the interaction level between the metal centers. However, is important to keep in mind that electrochemical results only give an insight on the delocalization and should not be used as a criteria to determine which class a system belongs to. Also, band-shape analyses of the ICT band are frequently complicated by multiple overlapping transitions.[75] The ICT band is observed in σ-bridged systems that are sufficiently flexible to allow the metal centers into close proximity, and is believed to arise from through-space coupling. In the case of π-bridged species, the NIR bands are more widely observed, even if the metals are well separated, suggesting a through-bond mechanism.[22]

3. Systems with Unsaturated Carbon Chain Bridges

Bimetallic and polymetallic systems that contain unsaturated hydrocarbon ligands with σ-bonded bridging metal centers are attracting considerable interest. They are commonly called "carbon σ-bonded molecular wires" and possess one-dimensional semirigid structures, which facilitates the electronic communication between the two redox active moieties.[13] As a result, potential applications for these systems have been suggested as molecular devices, electronic current rectifiers, and switches.[7,15,108,109]

The simplest bridge is a linear chain containing solely carbon atoms. To display intramolecular electronic communications, the systems must contain conjugated bridges able to promote delocalization. Hence, simple alkyl spacers are less suited for this matter. If a bimetallic complex presents mixed saturated and unsaturated bridges, the metals could be insulated due to the saturated (alkyl) spacer. $[(C_6F_5)\{Ar_2P(CH_2)_8PAr_2\}_2Pt]_2(C{\equiv}C)_4$ is an example where both Pt atoms are connected through two $Ar_2P(CH_2)_8PAr_2$ (alkyl) and one $(C{\equiv}C)_4$ chain (see Figure 9). The electronic interactions occur through the unsaturated chain. The alkyl spacers, which protect the Pt−$(C{\equiv}C)_4$−Pt fragment, act as an insulator.[110] Conjugated alkenes and alkynes are more interesting carriers for long-range metal−metal interactions.[20]

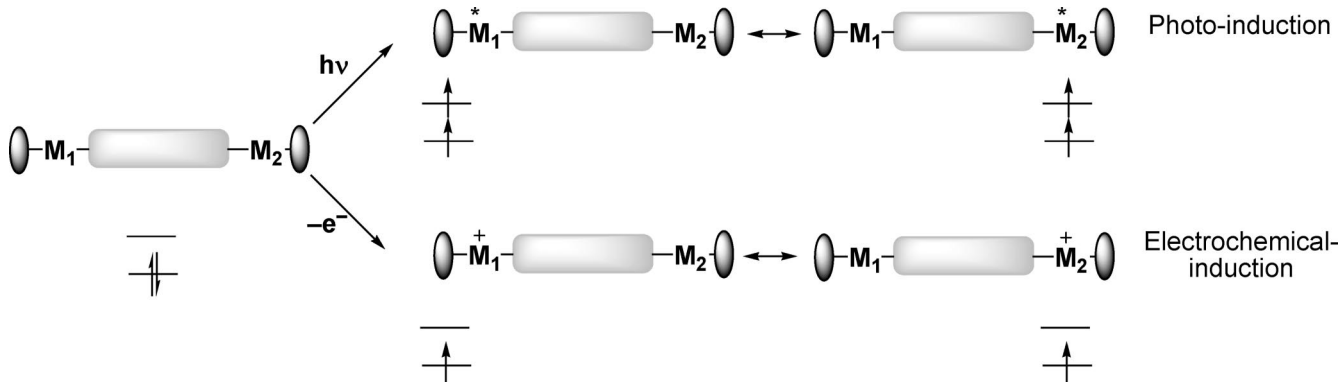

Figure 2. Electrochemical and photoinduced activation of a molecular wire.[13,20]

Purely organic molecular wires have been synthesized and have the advantage of being sufficiently soluble and stable to allow simple purification methods. They possess various unsaturated organic units and feature a conjugated π-electron network spread over the whole molecule. Impressive sizes up to 128 Å have been isolated.[13] Organometallic molecular wires have encountered synthetic problems such as decreased stability, which has often impeded their isolation and precluded their rapid development. The maximal lengths of the bridging ligand in these molecules are much smaller than the lengths of their purely organic homologues.[84,85]

Figure 2 represents the electron-transfer in molecular wires, whose mechanism can be activated by electrochemical or photoinduction.[111] However, very few of the potential synthesized molecular wires have been experimentally tested and evaluated for their electron conductivity. First and before considering a compound as a molecular wire, it is necessary to determine if the complex possesses the ability to convey electrons. For this, the electron conductivity can be directly measured through the bulk conductivity of the material or by studying the electronic interactions between the two metals utilizing electrochemistry (CV). When odd electron states are stable, UV−vis/NIR spectroscopy can produce decisive information on the strength of the coupling of the metal centers. Alternatively, in the presence of photoswitchable redox groups (photonic molecular wires), the study of electron-transfer can be achieved by time-resolved UV−vis spectrometry and fluorimetry. Finally, the direct measurement of the electron conductivity capability of a single molecule is also a useful technique to investigate this property. This method requires systems possessing a sufficient bridging length of at least 10 nm, mainly because of the type of instrument used.[13]

According to the molecular nature and structure of the bridging ligand, it is possible to classify molecular wires into three main groups: all-carbon sp-bridged, carbon-based sp^2-bridged and carbon-based sp/sp^2-bridged systems; these systems will be described in detail in the following sections.

3.1. All-Carbon sp-Bridged Systems

The most common examples of bimetallic complexes with linear unsaturated carbon chains such as LM−$(C\equiv C)_n$−ML are those with $n = 1$.[112–115] Higher homologues with $n = 2-10$ have also been synthesized.[116] Complexes with polyynediyl bridges LM−$(C\equiv C)_n$−ML comprise the most fundamental class of carbon-based wires.[117–120] To date, polyynediyl bridged complexes with $n = 1-8$, 10, 12, 14, 16, 20, 24, and 28 have been synthesized and isolated.[109,121] Among these dinuclear species, it is possible to distinguish between systems with an even or odd number of carbon atoms, with even numbers being by far the most commonly found.[20] The simple series HC_nH is only known for even values of n because of the different nature of the ground-states. An even value of n presents a stable closed shell singlet, whereas an odd value displays an unstable open shell triplet.[122]

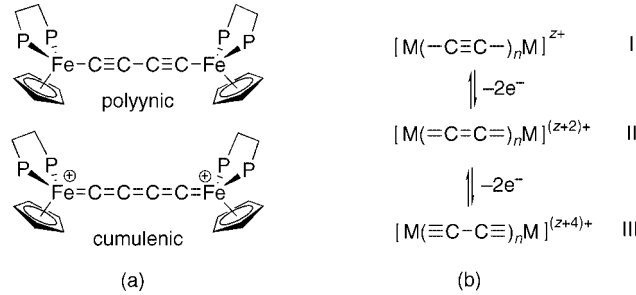

Figure 3. (a) Polyynic and cumulenic C_4 chains and (b) general three valence structures related by two-electron oxidations for C_n bridges with an even value of n.

Several C_4-bridged complexes show similar structures to those of butadiyne. Depending on the d^x electronic configuration, the C_4 chain presents either a cumulenic (oxidized) or polyynic (reduced) form. The interactions between the two metal centers can be expressed by three valence structures related to the C_4 bridge, which are related by two-electron oxidations as shown in Figure 3.[123]

DFT calculations performed on the family of complexes $[\{Cp(CO)_2M\}_2(\mu\text{-}C_n)]$ (M = Cr, Mn, Fe; $n = 4-8$) suggest that the geometrical structure is essentially determined by the nodal pattern of the highest molecular orbital of d_π-p_π character of the bridge. On the basis of these results, the authors have developed a simple molecular orbital model, which allows the estimation of the valence formulation in these specific type of dinuclear complexes on the basis of the d^x configuration of the metal and the separation of the different orbitals (σ, δ and π). If the δ-orbitals are not too high in energy, d^5 and d^7 display a polyynic structure (I and III, respectively), whereas d^6 is a cumulenic structure (II). When the δ-orbitals lie much higher in energy than the π-orbitals, only polyynic structures have been calculated.[116]

Only a few examples of systems having an odd number of C atoms in the bridge (length greater than one) are known, and they are mainly nonsymmetrical complexes (heterobimetallic or homometallic with different ancillary ligands).[20] The main reason is their difficult formation, because the coupling of C≡C building blocks is much easier and only leads to bridges with an even number of carbons. In general, for complexes with odd carbon bridges, two different valence

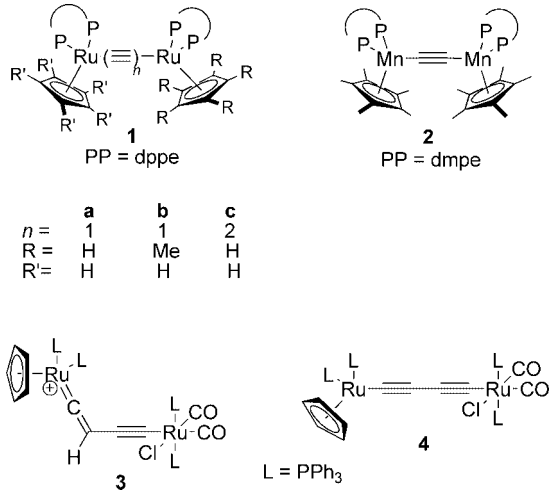

Figure 4. Homobimetallic complexes presenting different C_2, C_4, and C_4H carbon chains as linkers.

structures are possible: a symmetrical cumulenic structure M=C=(C=C)$_n$=M and a nonsymmetrical polyynyl/carbine structure M−(C≡C)$_n$−C≡M.[124] Complex [Cp(PPh$_3$)$_2$Ru-(C$_5$H)(PPh$_3$)$_2$Cp][BPh$_4$] is one of the few examples of homobimetallic systems (presenting the same ancillary ligands) that has an odd number of C atoms. However, in the solid state, it displays an unexpected nonsymmetrical structure of the form M=C=C=CH−C≡C−M.[125] Also, electrochemical measurements have shown that cumulenes with an odd number of carbons are electronically decoupled and therefore of no interest as potential conductors.[126]

A structural and chronological overview of all-carbon sp-bridged systems is presented from 2004 to 2009. The synthesis and study of the electronic properties of systems containing ethynyl bridges continues to be developed because of their interest as metal-supported fragments and possible use in nanoscale devices.[13,15] An increase in the electronic communicating properties could be achieved with electron rich phosphine-substituted ligands. Many homo- and heterometallic complexes of the type Cp^R(PP)M−(C≡C)$_2$−M(PP)Cp^R, with M = Fe, Ru, or Os and PP = (PPh$_3$)$_2$, dppm, or dppe (dppm = diphenylphosphinomethane and dppe = 1,2-diphenylphosphinoethane) and Cp^R = Cp if R = H, or Cp* if R = Me, have been synthesized and exhibit a variety of redox processes.[100] Electrochemical studies indicate that the presence of strong electron donating ligands results in a decrease in the oxidation potentials. These studies have also suggested that an efficient electronic communication between the two metal centers occurs through the carbon chain.

Figure 4 shows different examples of bimetallic complexes linked by ethynyl bridges (C_2 and C_4) and a C_4H bridge containing different ancillary ligands.

Table 1 displays electrochemical data for different C_2 and C_4 complexes. The large ΔE values found suggest electronic interactions between the metal centers for all these species. The diruthenium complex **1a** presents three reversible and one irreversible one-electron processes.[127] The low values of the first two events (E_1 and E_2) are consistent with the ease of the chemical oxidation of **1a** to **1a**$^+$ and to **1a**$^{2+}$. The oxidation potentials for **1a** and **1b** vary only slightly, even though **1b** has a more electron-donating group (Cp*).[127] Complex **1b** presents more anodic potentials relative to **1a**. However, the comparison is not evident as **1b** is an asymmetric system relative to **1a**. As the oxidation proceeds, structural data and DFT calculations show a gradual change from a ethynediyl (M−C≡C−M) structure (**1a**) to a cumulenic (M=C=C=M) structure (**1a**$^{2+}$). Hence, the oxidation causes the shortening of the M−C bonds and the lengthening of the "C−C" bonds. The authors claim that these studies, complemented by spectroscopic data, indicate a delocalization of charge over both Ru centers and the carbon chain.

The di-Ru complex **1c** is more difficult to oxidize than **1a** because of its longer carbon chain.[128] This is not surprising since the chain length is the only difference compared to complex **1a**. The decrease in metal−metal interactions is possibly due to the decreased coupling of the metal centers. Analogous complexes of **1c**, with the combinations of phosphine groups such as dppe and PPh$_3$, and with Cp and Cp* rings, confirmed the expectation of lower redox potentials values when strong electron-donating ligands are present. Cp(dppe)Ru−(C≡C)$_2$−Ru(PPh$_3$)$_2$Cp displays redox potentials at −0.22 and +0.42 V with a ΔE value of 640 mV, whereas Cp*(dppe)Ru−(C≡C)$_2$−Ru(PPh$_3$)$_2$Cp exhibits redox potentials at −0.33 and +0.34 V with a ΔE value of 670 mV.[128]

The dimanganese complex **2**$^{2+}$ displays three reversible one-electron processes.[129] The large ΔE values emphasize the existence of strong interactions between the Mn centers. The authors have attributed process E_1 to the couple Mn^{II}Mn^{II}/Mn^{II}Mn^{I} (**2**/**2**$^-$), E_2 to the couple Mn^{III}Mn^{II}/Mn^{II}Mn^{II} (**2**$^+$/**2**), and E_3 to the couple Mn^{III}Mn^{III}/Mn^{III}Mn^{II} (**2**$^{2+}$/**2**$^+$). The most cathodic process (E_1) has a very negative potential. Thus, this anion is difficult to synthesize by chemical processes. A detailed study based on DFT calculations, X-ray diffraction and CV emphasize, according to the authors, that in complex **2**, the Mn centers show strong electronic coupling and that the mixed-valence species **2**$^+$ belongs to the class III classification. However, as it was previously mentioned, DFT calculations can yield an erroneous result because it tends to overdelocalize the unpaired electron. Similar to that found for **1a**, as the oxidation state increases, there is a gradual change from ethynediyl to a cumulenic structure (M−C lengths = 1.872 Å for **2**, 1.792 Å for **2**$^+$ and 1.733 Å for **2**$^{2+}$), and **2**$^+$ has two equivalent Mn centers.

The di-Ru complex **3** (Figure 4) has been synthesized using the fragment C_4H, which is bound to one ruthenium center as a σ-alkynyl species and to the other as a vinylidene. Its structural conformation has been determined by ^{1}H and ^{13}C NMR studies. Also, the protonation of the butadiynediyl complex **4** exclusively regenerates complex **3** and not its

Table 1. Electrochemical Data for Several C_2 and C_4 Complexes[a]

complex	E_1 (V)	E_2 (V)	E_3 (V)	E_4 (V)	ΔE (mV)	ref
1a	−0.61	+0.21	+1.06	+1.74[b]	820/850/680	127
1b	−0.60	+0.22	+1.07		820/850	127
1c	−0.24	+0.35	+1.08	+1.44[b]	590/730/360	128
2^{2+}	−2.36	−1.38	−0.39		988/988	129

[a] All redox potentials are relative to [Cp$_2$Fe]$^+$/Cp$_2$Fe. [b] Irreversible.

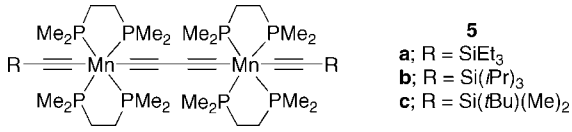

Figure 5. Bimetallic Mn complexes with a C_4 spacer.

Table 2. Electrochemical Data for 5a−c[a]

complex	E_1 (V)	E_2 (V)	ΔE (mV)
5a[b]	−0.84	−0.29	550
5b[b]	−0.86	−0.29	570
5c[b]	−0.85	−0.29	560

[a] All redox potentials are relative to $[Cp_2Fe]^+/Cp_2Fe$. [b] Data from ref 131.

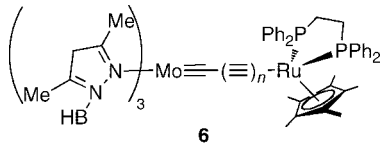

Figure 6. Complexes presenting bridges with odd number of carbon atoms.

Table 3. Electrochemical Data for 6a−c[a]

complex	E_1 (V)	E_2 (V)
6a[b]	+0.20	+0.73
6b[b]	+0.31	+0.75
6c[b]	+0.47	+0.84

[a] All redox couples are relative to $[Cp_2Fe]^+/Cp_2Fe$. [b] Data from ref 133.

tautomeric isomer $[Cl(CO)_2(L)_2Ru{=}C{=}CHC{\equiv}C{-}RuL_2Cp]$-$PF_6$.[130] Studies on their electronic properties have not been reported.

Berke et al.[131] have studied other bimetallic manganese complexes with a C_4 spacer (**5a−c**).The mixed-valence complexes $\mathbf{5a}^+$, $\mathbf{5b}^+$, and $\mathbf{5c}^+$ are synthesized by a coupling process using a C_4−Mn building block. These new compounds can be either fully oxidized to form $\mathbf{5a}^{2+}$, $\mathbf{5b}^{2+}$, and $\mathbf{5c}^{2+}$ or reduced to form **5a**, **5b**, and **5c** (Figure 5).

Table 2 displays the electrochemical data for **5a−c**. These studies suggest metal−metal interactions, with ΔE values of 550 mV for **5a**, 570 mV for **5b**, and 560 mV for **5c**. If experimental error is taken into account, it can be said that **5a−c** display the same ΔE values. Single crystal X-ray diffraction reveals two equivalent Mn centers for complex $\mathbf{5a}^+$ (Mn−C = 1.768 Å), suggesting a strong communication between the metal centers.

Complexes containing carbon chains with an odd number of carbons have electronic structures that require at least one M−C(bridge) forming a multiple bond. Since 2004, most of the examples of these types of complexes with a C_n (where n = odd number) bridge are heterobimetallic,[132] such as L−Mo≡C−(C≡C)−Ru−L (**6a**), L−Mo≡C−(C≡C)$_2$−Ru−L (**6b**), and L−Mo≡C−(C≡C)$_3$−Ru−L (**6c**) (Figure 6).[133]

In complexes **6a−c**, the redox potentials (E_1 and E_2) become more positive as the organic chain lengthens (Table 3). This reflects an increasing electron-transfer from the metal centers to the carbon chain. The authors have suggested that this is a result of the higher localization of the HOMO orbital on the carbon chain.[133] However, evidence for this suggestion has not been given.

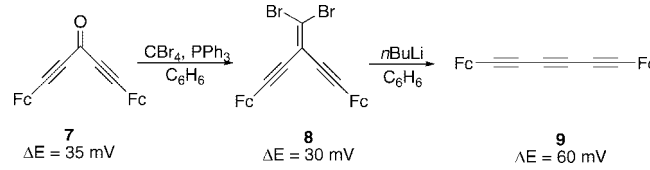

Figure 7. Synthesis of Fc−(C≡C)$_3$−Fc where Fc = $CpFe(C_5H_4)$.[137]

The monometallic Ru complex Cp*(dppe)Ru−(C≡CC≡CSiMe$_3$) has a E_1 value of +0.43 V.[133] Thus, the first redox process (E_1) on **6a−c** can be attributed to the Ru fragment. The monometallic Ru analogue and **6c** display a similar redox potential (E_1). This suggests an electronic isolation of the metal centers and no communication through the chain on **6c**.

Ferrocenyl polyynes of the type Fc−(C≡C)$_n$−Fc, where Fc = $CpFe(C_5H_4)$, have been prepared since the early 1970s and have been extensively reviewed by Low and Roberts.[11] Cowan et al.[134,135] have reported electrochemical studies for ferrocene polyyne complexes with n = 1 and 2. These systems present two processes with ΔE values of 130 and 100 mV, respectively. Their mixed-valence analogues are classified as class II systems. According to the authors, Fc−(C≡C)$_6$−Fc shows a two-electron oxidation process and hence the absence of electronic coupling by this method.[136] Figure 7 represents the species of the type Fc−(C≡C)$_3$−Fc synthesized by Ren et al.[137]

Complex **7** is converted to **9** by reaction of CBr_4 and in the presence of PPh_3. It can then react with nBuLi to form **9**. These three complexes have been studied by X-ray diffraction, displaying Fe···Fe distances of 9.72 Å for **7**, 10.55 Å for **9**, and 12.02 Å for **9**. Electrochemical studies of **7**-**9** exhibit quasi-reversible two-electron waves with ΔE values of 35, 30, and 60 mV, respectively. These values have been estimated using the Taube−Richardson model[138] because it is impossible to directly determine ΔE because of the quasi-reversible two-electron nature of the oxidation. Complex **9** presents the strongest electrochemical interaction despite having the longest Fe···Fe distance. The central C atom in complexes **7** and **9** results in less electrochemical interaction perhaps because of the less effective mediation of electronic coupling, resulting from the electronegative substituents bound to it (O for **7** and CBr_2 for **9**).

Several series of complexes with Pt−(C≡C)$_n$−Pt units (**10−13**, $PtC_{2n}Pt$) have been described by Gladysz et al.[110,139–141] Complexes of the type $PtC_{2n}Pt$ (n = 2−4, 6, 8, 10, 12, and 14) present thermal stabilities that can often exceed 200 °C, whereas organic polyynes with comparable chain lengths rapidly decompose at room temperature.[142] Figure 8 shows the structure of several types of $PtC_{2n}Pt$ systems.

UV−vis spectroscopy studies demonstrate more intense and red-shifted bands as the carbon length increases, which is indicative of electronic interactions.[140–143] Time-dependent DFT calculations suggest that the absorptions correspond to $\pi-\pi^*$ transitions that originate in the carbon chain and they are red-shifted with carbon length.[141] The CV studies show one quasi-reversible process for each complex, believed to involve one-electron in each case. The oxidation becomes thermodynamically more difficult and less reversible at longer chain lengths, as shown by the increasingly positive E_a (oxidation redox potential) and the decreasing i_c/i_a values, respectively (i_c and i_a denote cathodic and anodic currents,

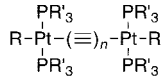

Complex	n	R	R'3
10	3-6, 8, 10, 12, 14	(*p*-tol)	(*p*-tol)$_3$
11	2-4, 6	C_6F_5	(*p*-tol)$_3$
12	4	Cl	(*p*-tol)$_3$
13	4	C_6F_5	**a**; Ph_2, {$(CH_2)_7$-CH_3}
			b; Ph_2, {$(CH_2)_9$-CH=CH_2}
			c; Ph_2, {$(CH_2)_4$-O-$(CH_2)_2$-CH=CH_2}

Figure 8. Structure of $PtC_{2n}Pt$ systems exhibiting different lengths (n) and substituents (R, R′).

Table 4. Electrochemical Data for Several $PtC_{2n}Pt$ Complexes[a]

complex		E_a (V)	i_c/i_a	ref
10a	PtC_6Pt	+0.86		142
10b	PtC_8Pt	+0.97		142
10c	$PtC_{10}Pt$	+1.09		142
10d	$PtC_{12}Pt$	+1.20		142
10e	$PtC_{16}Pt$	+1.26		142
10f	$PtC_{20}Pt$	+1.40		142
12	PtC_8Pt	+1.12	0.94	140
13a	PtC_8Pt	+1.30	0.68	231
13b	PtC_8Pt	+1.41	0.15	139
13c	PtC_8Pt	+1.31	0.72	139

[a] All samples recorded in CH_2Cl_2 solutions. All redox couples are relative to AgCl/Ag.

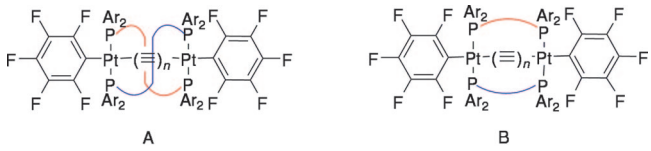

14

Figure 9. Two different conformations (A and B) for the family of complexes **14** (Ar = Ph, *p*-tol, *p*-C_6H_4-*t*Bu).

respectively, for the different types of complexes). Table 4 displays electrochemical data for several $PtC_{2n}Pt$ systems.

A new family of bridged systems [(C_6F_5){$Ar_2P(CH_2)_mPAr_2$}$_2Pt]_2(C{\equiv}C)_n$ (**14**, $PtC_{2n}Pt$-*m*/Ar) has been synthesized, which presents two different conformations depending on the length of the sp and sp^3 chains (Figure 9).[116,117]

In the family of complexes **14**, the crystal structures of **14d**−**g** and **j** show that the sp^3 chains wrap around the sp chain in a chiral double-helical conformation (A), yielding insulated molecular wires. They have potential uses as household insulated wires. At lower sp^3/sp carbon ratios, formally achiral conformations (B) are observed, such as **14a**−**c**, **h**, and **i**.[144] In general, the family of complexes **14** present thermodynamically less favorable oxidation potentials than their nonbridged analogues (**11**) but higher reversibility. Table 5 summarizes electrochemical data for the family of complexes **11** (nonbridged $PtC_{2n}Pt$) and **14** ($PtC_{2n}Pt$-*m*/Ar). They are also believed to undergo one-electron processes.

In the series of systems **14**, those with conformation A present higher reversibility than their corresponding B analogues with the same number of Pt−$(C{\equiv}C)_n$−Pt units. This has been attributed to their metal centers being more sterically shielded in the double-helical structure, stabilizing the radical cation. Unexpectedly, **14d** presents a lower reversibility compared to the analogue systems **14b** or **14c**. The authors have attributed this to the larger Ar group in **14d**, which labilizes the resulting cation.[144]

Table 5. Electrochemical Data for the Family of Complexes 11 and 14 (Nonbridged $PtC_{2n}Pt$ and $PtC_{2n}Pt$-*m*/Ar Systems, Respectively)[a]

complex		E_a (V)	i_c/i_a	conformation
11a[b]	PtC_4Pt	+0.94	0.98	
14a[b]	PtC_4Pt-8/Ph	+1.05	0.94	B
11b[b]	PtC_6Pt	+1.16	0.71	
14b[b,c]	PtC_6Pt-10/Ph	+1.25	0.82	B
14c[b,c]	PtC_6Pt-12/Ph	+1.23	0.84	B
14d[b,c]	PtC_6Pt-14/*p*-tol	+1.24	0.45	A
11c[c]	PtC_8Pt	+1.26	0.78	
14e[c]	PtC_8Pt-14/Ph	+1.31	0.78	A
14f[c]	PtC_8Pt-14/*p*-tol	+1.26	0.71	A
14g[c]	PtC_8Pt-14/*p*-C_6H_4-*t*Bu	+1.25	0.76	A
14h[c]	PtC_8Pt-10/Ph	+1.32	0.10	B
14i[c]	PtC_8Pt-11/Ph	+1.33	0.36	B
11d[c]	$PtC_{12}Pt$	+1.47		
14j[c]	$PtC_{12}Pt$-18/Ph	+1.47	0.35	A

[a] All samples recorded in CH_2Cl_2 solutions. All redox couples are relative to AgCl/Ag. [b] Data from ref 144. [c] Data from ref 110. [c] Data from ref 231.

3.2. Carbon-Based sp^2-Bridged Systems

While polyynediyl bridges are one of the most studied carbon-based molecular wires, few studies have been carried out with bimetallic polyenediyl bridges. Many conjugated organic materials such as polyacetylenes have only sp^2-hybridized carbon atoms and exhibit high electrical conductivity upon doping.[109,121] Consequently, polyenediyl bridges are also expected to present interesting properties. In fact, generally stronger coupling is found in mixed-valence complexes presenting polyenediyl bridges than those with polyynediyl bridges.[87,145–147] For alkenes, the HOMO and LUMO orbitals of the bridge are higher and lower in energy, respectively, compared to those for alkynes, therefore better placed energetically for overlapping with orbitals of the metal center. For example, Fc−$(CH{=}CH)_2$−Fc displays a ΔE value of 130 mV and λ_{max} of 1820 nm (ε_{max} = 1570 M^{-1} cm^{-1}),[148] whereas Fc−$(C{\equiv}C)_2$−Fc presents a ΔE value of 100 mV[135] and λ_{max} of 1180 nm (ε_{max} = 570 M^{-1} cm^{-1}).[135,149] The NIR data corresponds to the mixed-valence ions.

Sponsler et al.[150] have synthesized a series of conjugated diruthenium complexes by olefin metathesis for metal incorporation (OMMI). This method consists on effectively stopping the catalytic cycle after the first cycloreversion.[151] Consequently, the catalyst acts as a stoichiometric reagent and is incorporated into the product. Figure 10 illustrates both the general OMMI reaction and three di-Ru complexes (**15**−**17**, where Cy = cyclohexyl) synthesized using this method. Complexes with shorter bridges such as 1,3-butadiene, although theoretically stable, have not been successfully synthesized: attempts yielded only mono-Ru systems.[152]

Calculations have further indicated that the PCy_3 ligands are in close proximity, providing a steric shield around the bridge. Complexes **15** and **17** display similar oxidation potentials at +0.31 and +0.66 V and at +0.40 and +0.69 V, respectively (redox potentials are relative to $[Cp_2Fe]^+$/Cp_2Fe), meaning that conjugation and the size of the bridge has a small effect in the CV studies. However, the conjugated system **15** possesses a higher ΔE, consequently a higher metal−metal interaction. On the other hand, the authors have claimed that conjugation has a marked effect on reductions in these complexes, based on DFT calculations performed in $Cl_2(PPh_3)_2Ru{=}CH{-}CH{=}CH{-}CH{=}Ru(PPh_3)_2Cl_2$ (PH_3 analogue of **15**). These studies show that the LUMOs are

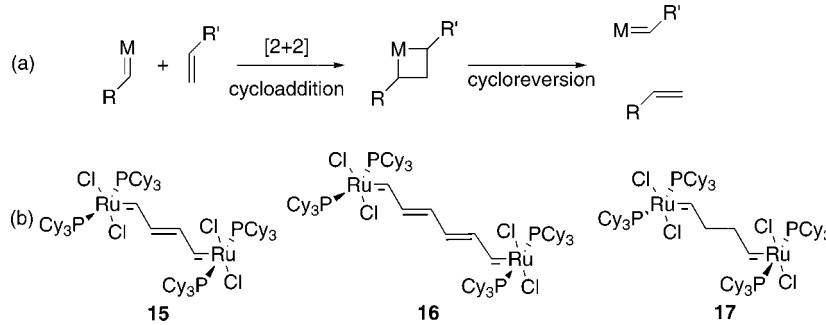

Figure 10. (a) General reaction method of OMMI; (b) di-Ru complexes synthesized by OMMI.

Table 6. UV−vis Data for Mono- and di-Ru Complexes[a]

compound	λ_{max} (nm)	ε_{max} (M^{-1} cm^{-1})	ref
$(PCy)_3RuCl_2{=}(CH{-}CH)_2{=}CH_2$	343	9600	150
15	438	17000	150
16	450	23000	150
17	very weak absorption		150
$[(NH_3)_5Ru(pz)]^{2+}$	472	13300	153
$[(NH_3)_5Ru(pz)Ru(NH_3)_5]^{4+}$	547	30000	153

[a] All samples recorded in CH_2Cl_2.

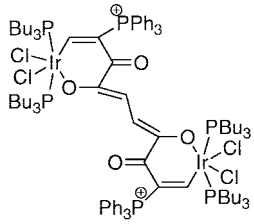

18

Figure 11. Structure of **18**.

associated with the π-bridged system, while the HOMO is not associated with the π-system. Complexes **15** and **17** display reduction potentials at −2.04 and −1.39 V and at −2.0 V (irreversible), respectively (redox potentials are relative to $[Cp_2Fe]^+/Cp_2Fe$).

Complex **16** presents a decreased stability of the oxidized and reduced forms in CV studies and no redox potentials have been obtained. A strong conjugation is observed in **15** and **16**, with strongly red-shifted and much more intense absorptions in the UV−vis spectra relative to their monometallic analogues and to **17**.[150] This has also been observed in the Creutz−Taube ion $Ru^{II}-Ru^{II}$ $[(NH_3)_5Ru(pz)Ru(NH_3)_5]^{4+}$,[153] which is shifted by 75 nm relative to the mononuclear Ru^{II} system (Table 6). The authors do not give any assignments for the bands observed. However, the shifts in the binuclear species **15** and **16** are caused by the presence of the second metal center, meaning that both metals are interacting, in some degree, through the bridge.

Xia et al.[154] have synthesized an interesting di-iridium complex (**18**). Figure 11 depicts its structure, which can be considered as either two Ir centers connected by a ten sp^2-carbon chain or as two planar six-membered rings containing Ir centers linked by a $-(CH)_2-$ bridge. The electrochemical data suggests electronic interactions between the redox centers, with a ΔE value of 750 mV and the thermodynamic stability of the transient intermediates $\mathbf{18}^+$ and $\mathbf{18}^{2+}$. These observations have been attributed to the conjugation and coplanarity of the bridging ligand.

To date, the longest linear sp^2 carbon chain $(CH)_n$ bimetallic complexes that have been produced are Ru−$(CH)_{10}$−Ru (**19**)[155] and Ru−$(CH)_{14}$−Ru (**20**).[121] The latter presents a distance between the two metal centers of 19.88 Å (Figure 12). Previous reported complexes are limited to those with linear bridges $(CH)_n$ ($n = 2$, 4−6 and 8).[109,121,155]

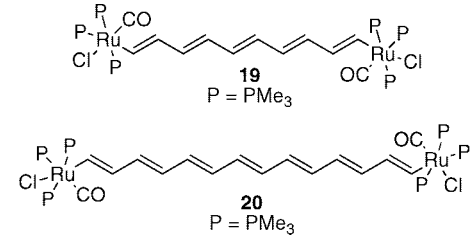

19
P = PMe_3

20
P = PMe_3

Figure 12. Structure of linear complexes **19** and **20**.

Table 7. Electrochemical Studies of di-Ru Systems[a]

complex	E_1 (V)	E_2 (V)	ΔE (mV)
19[b]	−0.01	+0.09	100
20[c]	+0.30	+0.50	200
Ru−$(CH)_6$−Ru[d]	−0.07	+0.31	380
Ru−$(CH)_8$−Ru[e]	−0.06	+0.18	240

[a] All complexes present quasi-reversible redox events and all redox potentials are relative to AgCl/Ag. [b] Data from ref 155. [c] Data from ref 121. [d] Data from ref 156. [e] Data from ref 157.

Table 7 summarizes the CV studies performed on di-Ru species. The electrochemical data confirm that **19** and **20** exhibit metal−metal interactions through their bridging ligand, with ΔE values of 100 and 200 mV, respectively. Similar complexes with smaller bridges, such as Ru−$(CH)_6$−Ru[156] and Ru−$(CH)_8$−Ru,[157] have ΔE values of 380 and 240 mV, respectively. As expected, the interactions decrease as the bridge lengthens. However, complex **20** displays a stronger metal−metal interaction relative to **19**. The reason behind this observation is unclear. Although ΔE is related to the thermodynamic stability of the mixed-valence systems, it also depends on other factors such as entropy, solvation, and through-space electrostatic interactions.[13,155]

Recent studies have classified certain type of bridging ligands as "non-innocent". This is because of their contribution to the electronic interaction of the metal centers, which is seen on their redox processes. Figure 13 shows the structure of complexes **21** and **22**, and Table 8 displays the electrochemical, IR and UV−vis/NIR data for these complexes that present non-innocent ligands.

For example, in the complex **21b**, the redox processes are dominated by the unsaturated organic ligand. As a consequence of the centered-ligand oxidations, this system does not display an ICT band in its mono-oxidized form. This was also observed for the 1,4-isomer **21a**. The *para*-substituted complex **21a** is more easily oxidized than the

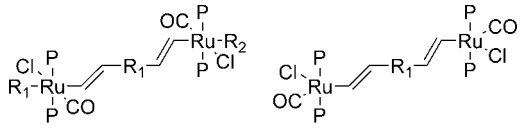

21
P = PPh_3
a; R_1 = 1,4-C_6H_4
R_2 = 4-EtOOCpy
b; R_1 = 1,3-C_6H_4
R_2 = 4-EtOOCpy

22
P = $PiPr_3$
a: R_1 = 1,4-C_6H_4
b; R_1 = 1,3-C_6H_4

Figure 13. Structure of complexes **21** and **22** (**a** and **b** for both).

meta-isomer **21b**. This is the result of the more effective conjugation through the bridge in the *para*-isomer. The oxidation of **21a** to **21a**$^+$ induces a small shift of the CO absorption band in the IR studies. In contrast, the oxidation of **21b** to **21b**$^+$ generates a two-band pattern. These observations suggest charge delocalization for **21a**$^+$ but partial charge localization on one styrylruthenium fragment for **21b**$^+$. This means that the latter presents inequivalent metal centers on the time scale of the IR experiment. The UV−vis/NIR data display transitions that closely resemble to those of partially oxidized or reduced pure organic ligand fragments, which is the result of the non-innocent nature of the bridging ligand.[158] Calculations have suggested that the occupied frontier orbitals correspond to antibonding interactions between the higher lying, nearly degenerate π-levels of the bridge and lower lying metal d_π orbitals. Therefore, changes on the metal moiety could lead to a more balanced electron distribution (decreasing the gap between the metal and the ligand orbitals) that will allow the study of the complexes by vibrational and electronic spectroscopy if the oxidized forms are stable. If the ruthenium moiety in complexes **21a** and **b** is changed to {($PiPr_3$)$_2$(CO)ClRu}, the gap is decreased and the oxidized forms **22a**$^+$ and **b**$^+$ present a greater metal character. Also, the partially and fully oxidized forms are stabilized by the ligand to a certain extent that they can be studied by electrochemistry and electronic spectroscopy.

Complexes **22a** and **b** display more cathodic potentials and greater ΔE values than their PPh_3 analogues **22a-PPh$_3$** and **22b-PPh$_3$**. The IR data for **22a** and **b** display a shift for the CO band upon the two oxidations with an overall value of approximately 70 cm^{-1}. This is larger if compared to the overall shift found for **21a** and **b** (45 cm^{-1}). This shows the higher contribution from the Ru centers to the redox orbitals of **22a** and **b**. However, these shifts could also be caused by the absence of the pyridine fragment which can serve to buffer the loss of electron density at the metal. The electronic spectra show new absorptions for the oxidized forms **22a**$^+$ and **22b**$^+$ which correspond to $\pi-\pi^*$ transitions and closely resemble the absorption obtained for the purely organic congeners. This means that the oxidation involves the bridging ligand.[158–160]

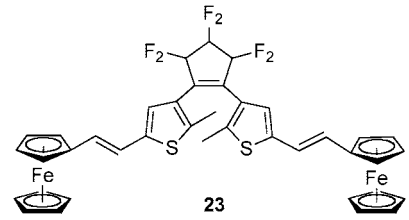

23

Figure 14. Two ferrocene units linked by a sp^2-bridge.

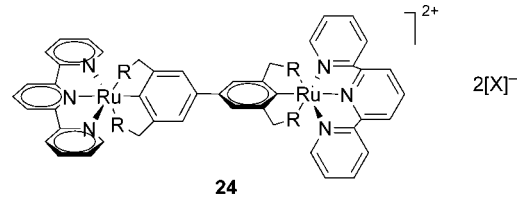

24
a; R = PPh_2, X = Cl
b; R = NMe_2, X = PF_6

Figure 15. Di-Ru complexes **24a** and **b**.

Figure 14 represents a bis(ferrocenyl) complex (**23**) that Liu et al.[161] have synthesized and characterized by X-ray diffraction. The system has a potential application in photoswitching devices because it displays photochromic properties.[162] However, metal−metal interactions, photochromism properties, and their effect on each other have not yet been reported for **23**.

Figure 15 displays two diruthenium complexes, [(tpy)Ru(PCP-PCP)Ru(tpy)]Cl$_2$ (**24a**) and [(tpy)Ru(NCN-NCN)Ru(tpy)]$_2$[PF_6]$_2$ (**24b**) (tpy = 2,2′:6′,2″-terpyridine). These have been synthesized and studied by van Koten et al.[163] Compounds **24a** and **b** are stable in air, moisture, and high temperatures, which may encourage the further development of these types of complexes.[163]

Table 9 shows selected electrochemical and UV−vis/NIR spectral data for the systems **24a** and **b**. Mixed-valence system **24a**$^+$ displays a broad absorption in the NIR region. This band has been deconvoluted into three Gaussian-shaped sub-bands. The observed $\Delta\bar{\nu}_{1/2(obs)}$ values for each transition are considerably lower than the calculated $\Delta\bar{\nu}_{1/2(calcd)}$, predicted by Hush theory for class II systems. The authors have

Table 8. Electrochemical, IR, and UV−vis Data for di-Ru Complexes[a]

	CV data			IR data	UV−vis data
complex	E_1 (V)	E_2 (V)	ΔE (mV)	$\nu_{C\equiv C}$ (cm^{-1})	λ_{max} (ε^b) (nm)
21a[c]	+0.02[e]	+0.36[e]		1926, 1727	257 (42), 300 (30), 350 (35), 410 (11)
21a$^+$ [c]				1939, 1729	341 (20), 585 (25), 1235 (30)
21a^{2+} [c]				1972, 1740	335 (22), 685 (20)
21b[c]	+0.24[e]	+0.56[e]		1926, 1711	275 (40), 290 (39), 410 (6.4)
21b$^+$ [c]				1963, 1941, 1714	410 (6.2), 586 (0.8), 1230 (1.3)
21b^{2+} [c]				1972, 1718	405 (6.8), 542 (1), 1900 (1.4)
22a[d]	−0.08	+0.18	260	1910, 1573, 1561	353 (10.3), 405 (2.6), 503 (1.3)
22a$^+$ [d]				1942, 1932, 1915, 1519, 1503, 1481	346, (5.8), 585 (4.2), 1255 (4.1)
22a^{2+} [d]				1991	266 (9), 430 (3.2), 624 (5.3)
22b[d]	+0.19	+0.46	270	1910, 1577, 1554	308 (16.6), 377 (4.7), 513 (0.8)
22b$^+$ [d]				1971, 1915, 1524	308 (15.3), 386 (3.5), 531 (1.8)
22b^{2+} [d]				1983	1265 (1.8), 2330 (0.5)
22a-PPh$_3$[d]	+0.18				
22b-PPh$_3$[d]	+0.31	+0.49	180		

[a] All redox potentials are relative to [Cp_2Fe]$^+$/Cp_2Fe. [b] Units of 10^3 M^{-1} cm^{-1}. [c] Data from ref 158. [d] Data from ref 159. [e] Cathodic peak.

Table 9. Electrochemical and UV−vis/NIR Spectral Data for Complexes 24a$^+$ and b$^+$ [a]

	CV data			UV−vis/NIR data					
complex	E_1 (V)	E_2 (V)	ΔE (mV)	λ_{max} (nm)	ε_{max} (M^{-1} cm^{-1})	$\bar{\nu}_{max}$ (cm^{-1})	$\Delta\bar{\nu}_{1/2(obs)}$ (cm^{-1})	$\Delta\bar{\nu}_{1/2(calcd)}$ (cm^{-1})	Γ
24a$^+$ [b]	−0.04	+0.13	170	1290	555	7751	2424	4231	0.43
				1609	1984	6215	1879	3789	0.50
				2066	3982	4840	1267	3343	0.62
24b$^+$ [b]	−0.25	−0.07	180	1875	33000	5333	1616	3509	0.70

[a] All redox potentials are relative to $[Cp_2Fe]^+/Cp_2Fe$. Compound **24a**$^+$ displays three bands in the UV−vis/NIR spectrum. [b] Data from ref 163.

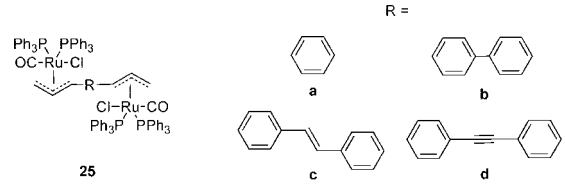

Figure 16. Di-Ru complexes **25a−d**. All the bridge phenyl fragments present a 1,4-binding.

classified **24a**$^+$ as a borderline class II/class III system because of the fairly low intensity of the bands, with their maxima being virtually independent of the solvent. The characteristic properties of phosphine groups (poor σ-donor and π-acceptor) attenuate the delocalization of the unpaired electron in the mixed-valence complex **24a**$^+$.

Mixed-valence system **24b**$^+$ presents an intense asymmetric band originating from two closely spaced electronic transitions (λ_{max} = 1875 nm with a shoulder at 1650 nm). The main absorption band at λ_{max} = 1875 nm is fairly narrow, highly intense and display negligible solvatochromism. Therefore, the authors have suggested that **24b**$^+$ is an intrinsically delocalized class III complex. Also, they have assigned the NIR bands to charge-transfer resonances bands rather than ICT transitions.

Figure 16 shows a series of conjugated di-allyls complexes of diruthenium presenting different bridging ligands (**25a−d**), synthesized by Liu et al.[164] Table 10 summarizes UV−vis and CV data for these complexes. They present long-wavelength transitions of strong intensity, corresponding to MLCT bands. The energy absorption decreases in the order **25b** > **25d** > **25a** > **25c**. They also display additional very strong (ε > 44000 M^{-1} cm^{-1}) high-energy bands at around 240 nm which probably correspond to intraligand transitions. Electrochemical studies suggest that **25a** displays a moderate electronic interaction between the metal centers, implying it might correspond to a class II mixed-valence complex. Complex **25c** presents a longer bridging ligand, which is responsible for the weaker metal−metal interaction relative to **25a**. Complexes **25b** and **d** display irreversible processes and the absence or nearly negligible interaction of the metal centers through the ligand.

Figure 17 displays a series of dicobalt complexes of tetramethyleneethane (TME) that have been recently synthesized.[165] The ligand is capable to adjust its binding capability according to the oxidation state of the metal center

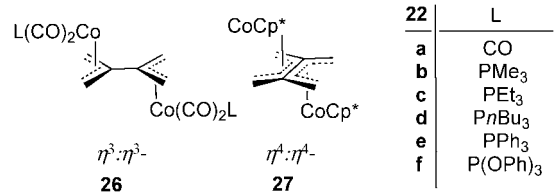

Figure 17. Di-Co complexes of TME **26a−f** and **27**.

Table 11. Electrochemical Data for Complexes 26a−f and 27[a]

complex	E_1 (V)	E_2 (V)	ΔE (mV)
26a[b]	+0.25[c]	+0.50[c]	250
26b[b]	−0.07[c]	+0.15[c]	220
26c[b]	−0.27[c]	+0.03[c]	300
26d[b]	−0.21[c]	+0.07[c]	280
26e[b]	−0.03[c]	+0.39[d]	
26f[b]	−0.05[c]	+0.36[d]	
27[b]	−0.93[c]	−0.47[d]	

[a] All redox potentials are relative to $[Cp_2Fe]^+/Cp_2Fe$. [b] Data from ref 232. [c] Quasi-reversible. [d] Irreversible oxidation.

and the ancillary ligands. X-ray diffraction studies demonstrate that the family of complexes **26** presents Co^I centers and a η^3:η^3-configuration, whereas **27** has Co^{II} centers and a η^4:η^4-configuration. All these systems present metal−metal interactions through the delocalized bridging ligand.

For the family of complexes **26**, the electronic communication within the metal centers can be studied relative to the electron-donating properties of the L group. CV studies display two quasi-reversible processes when L = PMe_3, PEt_3, and $PnBu_3$. However, when R = PPh_3 or $P(OPh)_3$, one quasi-reversible and an irreversible oxidation are observed. The degree of metal−metal interactions for these systems follows the trend PEt_3 > $PnBu_3$ > CO > PMe_3 > PPh_3 ≈ $P(OPh)_3$. Complex **27** also displays a quasi-reversible and an irreversible oxidation processes. Table 11 illustrates the CV data for the family of complexes of TME (**26a−f** and **27**).

3.3. Carbon-Based sp/sp^2-Bridged Systems

This section contains examples of systems containing mixed bridging ligands with either ethynyl and ethenyl carbon chains or ethynyl and an aromatic ring carbon chains.

A series of diruthenium and di-iron complexes with sp/sp^2 carbon chains as linkers have been synthesized (**28−31**).[62,166] Several studies on the family of complexes **28**

Table 10. Electrochemical and UV−vis Spectral Data for Complexes 25a−d[a]

	CV data			UV−vis data			
complex	E_1 (V)	E_2 (V)	ΔE (mV)	λ_{max} (nm)	ε_{max} (M^{-1} cm^{-1})	λ_{max} (nm)	ε_{max} (M^{-1} cm^{-1})
25a[b]	+0.26	+0.43	170	239	44300	396	21700
25b[b]	+0.33			240	61700	380	36500
25c[b]	+0.31	+0.42	110	240	52000	406	45300
25d[b]	+0.30			240	58100	389	45500

[a] All redox potentials are relative to $[Cp_2Fe]^+/Cp_2Fe$. [b] Data from ref 164.

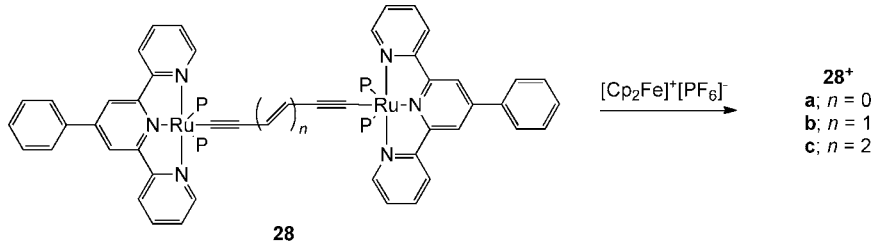

28
P = PPh_3
a; *n* = 0
b; *n* = 1
c; *n* = 2
d; *n* = 3

Figure 18. Di-Ru complexes bridged by sp/sp^2-carbon chains in the family of complexes **28a−d** and the formation of their mixed-valence analogues **28**$^+$**a−c**.

Table 12. Electrochemical and UV−vis/NIR Data for Complexes of the Type 28[a]

	CV data				MV	UV−vis/NIR data[c]			
complex **28**[b]	E_1 (V)	E_2 (V)	ΔE (mV)	K_c	**28**$^+$	λ_{max} (nm)	ε_{max} (M^{-1} cm^{-1})	$\bar{\nu}_{max}$ (cm^{-1})	Γ
a	−0.28	+0.33	610	2.50×10^{10}	**a**	1005	38810	9950	0.5
b	−0.21	+0.06	270	2.48×10^{4}	**b**	1069	14310	9354	0.4
c	−0.18	−0.02	200	6.15×10^{2}	**c**	1171	6850	8540	0.1
d		−0.09	<70						

[a] All redox potentials are relative to $[Cp_2Fe]^+/Cp_2Fe$. [b] Data from ref 62. [c] Correspond to the ICT bands, and data for the MLCT bands is not given.

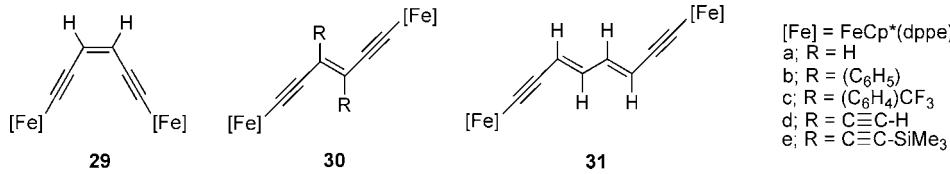

29 30 31

Figure 19. Series of di-Fe complexes **29−31**.

(Figure 18) have been executed to demonstrate the effect of increasing the number of ethenyl fragments on the electronic communication between the metal centers.

In the family of complexes **28**, the π-acceptor ability of the bridging ligand is enhanced as the number of ethenyl segments is increased, reducing the π-electron density of the Ru centers. Table 12 represents electrochemical and UV−vis/NIR data for the family of complexes **28**. The CV data demonstrate that the communication of the metals reduces dramatically with increasing number of ethenyl fragments with ΔE values of 610 mV for **28a**, 260 mV for **28b**, 165 mV for **28c**, and less than 70 mV for **28d**. It is similarly more difficult to achieve the first oxidation events and UV−vis spectroscopy studies show a large shift of the MLCT bands to higher energies (380−630 nm, $d_\pi(Ru) \rightarrow \pi^*$(ancillary ligand)). The π-electron-accepting ability in the bridging ligand is enhanced when the ethenyl bridge increases, which would reduce the π-electron density of the Ru^{II} centers and lower the energy of the $d_\pi(Ru)$ orbital. Therefore raising the energy gap between $d_\pi(Ru)$ and π^* orbitals (ancillary ligand), which induces a blue shift of the MLCT band. Mixed-valence systems of the family **28**$^+$ present strong ICT bands in the UV−vis/NIR spectrum, which the authors have attributed to the electronic transitions from the Ru^{II} to Ru^{III} centers. These redox and absorption spectral features, such as a large K_c, high intensity of the ICT band, narrow half-width ($\Delta\bar{\nu}_{1/2}$) and solvent independency of the ICT band, suggest that complex **28a**$^+$ corresponds to a class III system. However, in this case, the ICT band corresponds to the transition from one delocalized state to another and not from Ru^{II} to Ru^{III} centers. Complex **28b**$^+$ exhibit broader and weaker ICT bands compared to **28a**$^+$ and a lower K_c value, implying it is a borderline class II/class III system. A much weaker and broader ICT band and a lower K_c value for **28c**$^+$ compared to the other two, corresponds to a class II species.

Analyses on the family of complexes **29−31** (Figure 19) have been performed to show the effect on the electronic delocalization when adding substituents to the ethenyl fragment.[166,167] Table 13 summarizes the electrochemical and UV−vis/NIR data for the family of complexes **29−31**.

The series of complexes **29−31** present two reversible one-electron redox waves and very large K_c values (10^8-10^9), except for **31** (10^4). Indeed, its bridge is longer and possesses more ethenyl fragments. As mentioned earlier, K_c is expected to diminish exponentially as a function of the distance between the metal centers. The series of complexes **29−31** are suggested to correspond to class III systems not only by their electrochemical behavior (large K_c constants) but also by their intense absorptions in the UV−vis/NIR attributed to ICT bands. Their $\Delta\bar{\nu}_{1/2(obs)}$ values are also narrower than the critical bandwidth $\Delta\bar{\nu}_{1/2(calcd)}$. The study by Akita et al.[166] showed that the substituents R have a considerable effect on the delocalization on the systems of the type **30**, and follows the order C_6H_5 (Ph) > C≡C−H, C≡C−$SiMe_3$ > H. The Ph group leads to an enhanced delocalization of the odd electron over the π-system compared to the other substituents. When CF_3 groups are introduced to the Ph group (**30c**), their electron-withdrawing properties shift the redox potentials to more positive values. However, this system still presents very high K_c values, meaning that the radical species are not destabilized with respect to disproportionation by the CF_3 groups.

Table 13. Electrochemical and UV−vis/NIR Data for Complexes 29−31[a]

	CV data				UV−vis/NIR data for monocation			
	E_1 (V)	E_2 (V)	ΔE (mV)	K_c	$\bar{\nu}_{max}$ (cm^{-1})	ε_{max} (M^{-1} cm^{-1})	$\Delta\bar{\nu}_{1/2(obs)}$ (cm^{-1})	$\Delta\bar{\nu}_{1/2(calcd)}$ (cm^{-1})
29[b]	−0.99	−0.51	480	1.2×10^8	6305	16000	2488	3961
30a[b]	−1.02	−0.53	490	2.1×10^8				
30b[b]	−1.09	−0.56	530	1.4×10^9	6427	22000	1905	3853
30c[b]	−0.97	−0.42	550	3.0×10^9	6266	19000	1769	3805
30d[b]	−0.91	−0.41	500	2.7×10^8	5695	2270	2675	3627
30e[b]	−0.93	−0.41	520	6.8×10^8	5910	13200	2249	3695
31[b]	−0.87	−0.60	270	4.7×10^4	5181	5650	2664	3459

[a] All redox potentials are relative to $[Cp_2Fe]^+/Cp_2Fe$. [b] Data from ref 166.

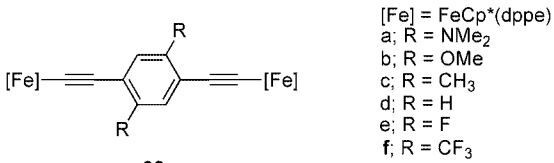

32

Figure 20. Series of di-Fe complexes **32**.

Akita et al.[168] have recently published another study regarding complexes of the type [Fe]−C≡C−*p*-$C_6H_2X_2$−C≡C−[Fe] (**32a**−**f**), where X = NMe_2, OMe, CH_3, H, F, CF_3 and [Fe] = FeCp*(dppe) (Figure 20). Similar to their previous studies, they have determined the effect of the substituents on the phenyl rings relative to the metal−metal interactions, finding that electron-donating substituents enhance the electronic delocalization through the bridge as seen by the electrochemical studies. Electron-donating substituents should increase the electron density at the metal centers in the neutral species, making the oxidation easier. The monocation species could be stabilized by the electron-donating groups, which should cause an anodic shift of the second oxidation process. This results in an increase of ΔE values. UV−vis/NIR studies show that $\Delta\bar{\nu}_{1/2(obs)}$ values are significantly smaller than the $\Delta\bar{\nu}_{1/2(calc)}$ values, suggesting that all these systems belong to class III. Table 14 displays electrochemical and UV−vis/NIR data for the family of complexes **32a**−**f**.

Figure 21 shows a series of diruthenium complexes with C_7, C_9, and $C_2C_6H_4C_2$ sp/sp^2-bridges that have been synthesized by Rigaut et al. (**33a**−**d**) and Low et al. (**34a** and **b**).[169] The authors have claimed that EPR, UV−vis/NIR, DFT, and CV studies on C_7 systems (**33a**−**c**) establish that in the reduced state (neutral species), the single electron is delocalized over the carbon chain with very small metal contribution. However in the oxidized form (dication), the odd electron is fully delocalized over the chain and the metal centers, over a distance of almost 12 Å, corresponding to class III systems.

Table 15 summarizes the electrochemical and UV−vis studies for the family of complexes **33**. The C_9 system **33d** presents red-shifted absorption bands in the UV−vis spectrum relative to the analogue **33a**. They are consistent with a longer conjugation pathway. Electrochemical studies show a smaller ΔE value than **33a**−**c**. The UV−vis and CV data agree with a weaker interaction of the metals on **33d** because of its longer bridging ligand relative to that of **33a**−**c**.

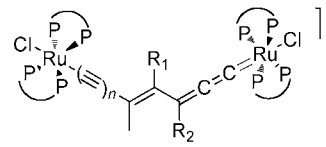

33
PP = dppe
(*n* = 1) **a**; R1 = H, R_2 = CH_3
b; R_1 = H, R_2 = Ph
c; R_1 = CH_3, R_2 = Ph
(*n* = 2) **d**; R_1 = H, R_2 = CH_3

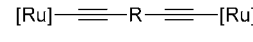

34
R = 1,3-C_6H_4
a; Ru = *trans*-Ru(dppe)$_2$Cl
b; Ru(dppe)Cp*

Figure 21. Structure for di-Ru complexes with C_7 and C_9 sp/sp^2-bridge carbon chains (**33a**−**d** and **34a**−**b**).

Table 15. Electrochemical and UV−vis Data for Complexes 33a−d[a]

	CV data			UV−vis data
complex	E_1 (V)	E_2 (V)	ΔE (mV)	λ_{max} (ε_{max}[b]) (nm)
33a[c]	+0.31	+0.99	680	455 (4.0); 710 (12.8)
33b[c]	+0.32	+0.97	650	494 (4.7); 746 (98.0)
33c[c]	+0.23	+1.06	830	502 (7.6); 764 (10.9)
33d[c]	+0.42	+0.96	540	526 (14.6); 744 (46)

[a] All redox potentials are relative to $[Cp_2Fe]^+/Cp_2Fe$. [b] Units of 10^3 M^{-1} cm^{-1}. [c] Data from ref 169.

Another example of complexes presenting non-innocent ligands are 1,3-{*trans*-Cl-(dppe)$_2$RuC≡C}$_2$$C_6H_4$ (**34a**) and 1,3-{Cp*(dppe)RuC≡C}$_2$$C_6H_4$ (**34b**) (Figure 21). Table 16 displays IR, electrochemical, and UV−vis data for complexes **34a** and **b** and their monometallic analogues. IR data on the mono-oxidized systems $\mathbf{34a}^+$ and $\mathbf{b}^+$ show two bands, which approximate to a superposition of the $\nu_{(C\equiv C)}$ bands for the monometallic complexes *trans*-RuCl(C≡CPh)(dppe)$_2$ and its monocation and Ru(C≡CPh)(dppe)Cp* and its monocation, respectively, which are also non-innocent systems. The electrochemical data suggest the thermodynamic stability of $\mathbf{34a}^+$ and $\mathbf{b}^+$ by means of the ΔE and K_c values obtained.

Table 14. Electrochemical and UV−vis/NIR Data for Complexes 32a−f[a]

	CV data			UV−vis/NIR data			
complex	E_1 (V)	E_2 (V)	ΔE (mV)	$\bar{\nu}_{max}$ (cm^{-1})	H_{ab}[d] (eV)	$\Delta\bar{\nu}_{1/2(obs)}$ (cm^{-1})	$\Delta\bar{\nu}_{1/2(calcd)}$ (cm^{-1})
32a[b]	−0.90	−0.57	330	4554 (21.8[c])	0.282	1022	3243
32b[b]	−0.84	−0.53	310	4570 (21.6[c])	0.283	1310	3249
32c[b]	−0.80	−0.52	280	4100 (17.5[c])	0.254	1750	3077
32d[b]	−0.76	−0.50	260	5100 (8.7[c])	0.316	1350	3432
32e[b]	−0.71	−0.42	290	4150 (15.5[c])	0.257	1250	3096
32f[b]	−0.67	−0.38	290	4080 (13.8[c])	0.253	1620	3070

[a] All redox potentials are relative to $[Cp_2Fe]^+/Cp_2Fe$. [b] Data from ref 168. [c] ε, in 10^3 M^{-1} cm^{-1}. [d] Calculated with expression $H_{ab} = \bar{\nu}_{max}/2$.

Table 16. IR ($\nu_{C\equiv C}$), Electrochemical, and UV−vis Data for Mono- and di-Ru Complexes[a]

		CV data			UV−vis data
complex	IR data (cm^{-1})	E_1 (V)	E_2 (V)	ΔE (mV)	$\bar{\nu}$ (ε^c) (cm^{-1})
34a[b]	2063	+0.43	+0.62	190	31350 (43.5)
34a^{+} [b]	2049			($K_c = 1600$)	17300 (2.8), 12120 (7.8), 9100
	1905				(1.2), 5800 (0.3), 3750 (0.9)
34a^{2+} [b]	1909				17000 (3.4), 11900 (9.4), 8800 (1.8)
34b[b]	2063	+0.18	+0.34	160	31500 (13)
34b^{+} [b]	2060			($K_c = 500$)	17800 (0.5), 14000 (1), 7750 (0.1),
	1934				4800 (0.1)
34b^{2+} [b]	1938				17400 (1.3), 13500 (2.3), 7500 (0.3), 4300 (0.1)
trans-RuCl(C≡CPh)(dppe)$_2$[b]	2075	+0.47	+1.31[d]		38450 (50), 31350 (23)
[*trans*-RuCl(C≡CPh)(dppe)$_2$]$^{+}$ [b]	1910				16900 (1), 12040 (10), 9080 (0.5)
Ru(C≡CPh)(dppe)Cp*[b]	2072	+0.25	+1.09[d]		29500 (95)
[Ru(C≡CPh)(dppe)Cp*]$^{+}$ [b]	1929				21100 (4.3), 11200 (5.1), 8100 (0.6)

[a] All redox potentials are relative to $[Cp^*_2Fe]^+/Cp^*_2Fe$. [b] Data from ref 170. [c] Units in 10^3 M^{-1} cm^{-1}. [d] Irreversible (anodic peak).

Table 17. Electrochemical Data for the Family of Complexes 35a−e, 36a, b, and d[a]

complex	E_1 (V)	E_2 (V)	ΔE (mV)
35a[b]	−0.18	+0.07	250
35b[b]	−0.06	+0.07	130
35c[b]	−0.07	+0.00	70
35d[b]	+0.03	+0.25	220
35e[b]	+0.15	+0.24	90
36a[c]	−0.20	+0.11	310 ($K_c = 1.5 \times 10^5$)
36b[c]	−0.24	+0.06	300 ($K_c = 1.5 \times 10^5$)
36d[d]	−0.51	−0.22	280 ($K_c = 5.4 \times 10^4$)

[a] All redox potentials are relative to $[Cp_2Fe]^+/Cp_2Fe$. [b] Data from ref 171. [c] Data from ref 172. [d] Data from ref 173.

The UV−vis/NIR data for the monocations display weak absorptions that can be deconvoluted into two Gaussian-shaped bands. DFT studies have suggested that they correspond to a charge-transfer band arising from the transition from a metal acetylide donor to a metal phenylacetylide acceptor and to a transition between d_π(Ru) orbitals and π(C≡C) orbitals. Therefore, the stabilization of the monocation arises from the delocalization of the unpaired electrons between one metal center, the acetylide fragment, and the aromatic ring. This is contrary to what is usually expected in mixed-valence systems, where the stabilization is given by the delocalization of the charge between the two metal centers. In conclusion, the electronic properties of complexes **34a** and **b** are significantly influenced by the oxidized ligand.[170]

Electronic communications through the bridge containing ethenyl and ethynyl fragments in other di-Ru species **35a−f** and **36a−f** have also been investigated.[171,172] Table 17 presents CV studies for **35a−e** and **36a**, **b**, and **d**, which demonstrate that the electronic communication decreases when the number of ethenyl fragments increases in the bridge. Chen et al.[171] have studied complexes that presented ethenyl bridges of the type 1,4-phenylene and 2,5-thienylene (C_4H_2S) rings (**35a−e**). Figure 22 illustrates the structures of complexes **35a−e**.

Rigaut et al.[15,172] and Field et al.[173] have studied systems that presented one Ph group as the ethenyl fragment and different metal fragments (**36a−f**, Figure 23). Some of these systems also present electronic interactions, as determined by electrochemical studies. No electrochemical data has been reported for **36c, e**, and **f**.

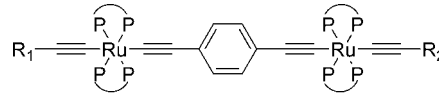

36
a-b; PP = dppe
c-f; PP = dmpe

a; $R_1 = R_2 = 1,4\text{-}C_6H_4CN$
b; $R_1 = H$, $R_2 = 1,4\text{-}C_6H_4CN$
c; $R_1 = R_2 = Ph$
d; $R_1 = R_2 = t$Bu
e; $R_1 = Ph$, $R_2 = t$Bu
f; $R_1 = t$Bu, $R_2 = C_6H_3\text{-}3,5\text{-}(t\text{Bu})_2$

Figure 23. Structure of di-Ru complexes **36a−f**.

Table 18 displays CV and UV−vis/NIR data for complexes **37** and **38**. This complexes display several ethenyl and ethynyl fragments connecting two Ru(dppe)$_2$Cl moieties (Figure 24).[174] Electrochemical studies show two one-electron reversible oxidation steps followed by a third irreversible oxidation (+0.84 V) for **37**. Complex **38** only displays one reversible oxidation wave which corresponds to a 1.9-electron process. The authors have suggested that these waves should be considered as two coinciding one-electron waves because of noncoupling of the two individual redox processes at each metal center. Another irreversible oxidation is also observed at 0.80 V. UV−vis/NIR data show absorption bands for **37**$^{+}$. The authors have claimed that the long-wavelength band cannot be assigned to an ICT band since the observed intensities are too high for such a weakly coupled system as assumed from electrochemistry. However, the calculated and observed bandwidths are in better agreement for a class II system. Is important to remember that electrochemical studies cannot be used on their own to classify a complex. No bands were observed for **38**$^{+}$. This supports the results obtained

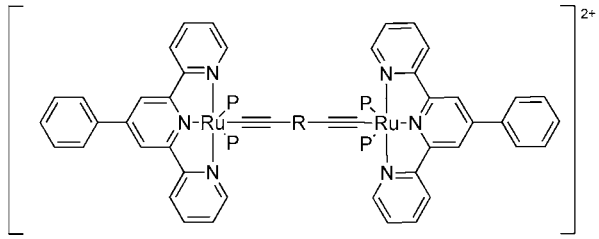

35
P = PPh_3
a; R = 2,5-(C_4H_2S)
b; R = [2,5-(C_4H_2S)]$_2$
c; R = [2,5-(C_4H_2S)]$_3$
d; R = 1,4-C_6H_4
e; R = 1,4-(C_6H_4)$_2$

Figure 22. Structure of di-Ru complexes **35a−e**.

Table 18. Electrochemical and UV−vis/NIR Data for the Complexes 37 and 38[a]

	CV data				UV−vis/NIR data for MV species		
complex	E_1 (V)	E_2 (V)	ΔE (mV)	K_c	$\bar{\nu}_{max}$ (cm^{-1}) (ε)[c]	$\Delta\bar{\nu}_{1/2(obs)}$ (cm^{-1})	$\Delta\bar{\nu}_{1/2(calcd)}$ (cm^{-1})
37[b]	+0.04	−0.03	70	10.8	5882 (230)	3860	3686
38[b]		+0.01					

[a] All redox potentials are relative to $[Cp_tFe]^+/Cp_2Fe$. [b] Data from ref 174. [c] In M^{-1} cm^{-1}.

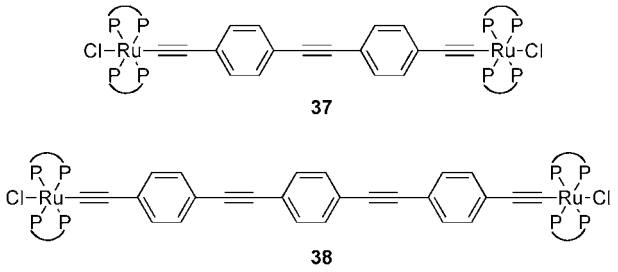

Figure 24. Structure of di-Ru complexes **37** and **38**.

from the CV studies. There is no apparent connection between both ruthenium centers and they are both oxidized independently at the same potential.

Figure 25 illustrates complexes **39a−f** that have been synthesized and studied by several authors.[175−182] Studies on metal−metal interactions for complex **39f** have not been reported.

The electrochemical studies of these electron-rich systems reveal two one-electron redox processes for **39a** and **b** with ΔE values of 290 and 220 mV, respectively. This is indicative of electronic communications between metal centers through the bridge. Complex **39c** displays only one reversible process. The introduction of the biphenyldiyl fragment **c** severely reduces the communication of the metals and the mixed-valence species $\mathbf{39c}^+$ is not stable. Complexes **39d** and **e** show two chemically reversible oxidation waves separated by 280 and 360 mV ($K_c = 1.3 \times 10^6$), respectively.

The authors have claimed that IR, UV−vis/NIR, and DFT studies indicate that the cation $\mathbf{39a}^+$, $\mathbf{d}^+$, and $\mathbf{e}^+$ correspond to a class III system (Table 19).Complex $\mathbf{39b}^+$ has also been assigned to class III, according to electrochemical studies. This could be arguable considering that electrochemical studies only give an insight of the interactions between the two metal centers but does not allow classification of the system according to Robin and Day classification. Also, DFT studies are not a reliable tool to properly assign a system to a specific class. The Cp* analogues have been previously synthesized by Lapinte and Paul.[13,176,180] Their mixed-valence species present higher thermodynamic stability of the corresponding monocation intermediate with respect to disproportionation than the family of complexes **39a−c**. This is probably the result of the enhanced electron-donating effect of the Cp* relative to Cp, which stabilize the positive charge on the metal groups.

Table 19. IR ($\nu_{C\equiv C}$) and UV−vis/NIR Data for the Family of Complexes 39[a]

		UV−vis/NIR (cm^{-1})	
complex	IR (cm^{-1})	$\Delta\bar{\nu}_{1/2(obs)}$	$\Delta\bar{\nu}_{1/2(calcd)}$
39a[b]	2031		
$\mathbf{39a}^{+}$ [b]	1981	1000[d]	3630
$\mathbf{39a}^{2+}$ [b]	1929		
39d[c]	2053		
$\mathbf{39d}^{+}$ [c]	1969, 1925	1430[e]	3770
$\mathbf{39d}^{2+}$ [c]	1972, 1952		
$\mathbf{39e}^{+}$ [d]		1660[f]	3170

[a] IR data measured in CH_2Cl_2. [b] Data from ref 175. [c] Data from ref 182. [d] Data from ref 177. [e] In CH_3CN. [f] In CH_2Cl_2.

Sita et al.[183] have recently reported a study on diferrocene frameworks (**40** and **41**), having end-to-end distances of ~4 nm (Figure 26). Table 20 summarizes the CV studies for the family of complexes **40** and **41**. The complex **40a** exhibits a single redox feature, presumably because of the unresolved redox process of both ferrocene centers, indicating a very poor or nonexistent interaction of the metal centers through the bridge. Also, the electron-withdrawing character of the substituents shifts, not very significantly, the redox couple to higher redox potentials compared to the unsubstituted-**40a** analogue ($R_1 = R_2 =$ H, +0.84 V). When a positive charge is placed on the system (**41a**), two processes are now observed at +1.04 and +1.23 V with a ΔE value of 190 mV. Complex **40b** shows two resolved redox waves because of its asymmetry at +0.86 and +0.99 V ($\Delta E = 130$ mV). However, when a positive charge is introduced to the system (**41b**), the separation of the two redox processes is 310 mV (+0.95 and +1.26 V). Therefore, the electronic communication of the substituted-ferrocene fragments is influenced by the pyridinium cation and also by the electron-withdrawing nature of the substituents.

However, it might be important to note that both **41a** and **b** are, in fact, fundamentally unsymmetrical because of the different bonding of the pyridine fragment with respect of the ferrocene fragments, such as **40a** and **b**. So in both cases, ΔE reflects the inherent inequivalence of the two Fe centers as well as any interactions. Indeed, the inequivalence is expected to be more significant in **41a** and **b** because the ferrocene on the left-hand side is in direct (*ortho*) conjugation with a good π-acceptor group (the pyridinium cation),

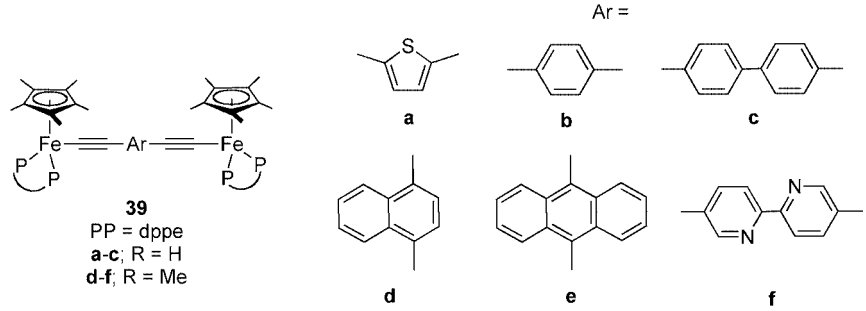

Figure 25. Di-Fe complexes **39a−f**.

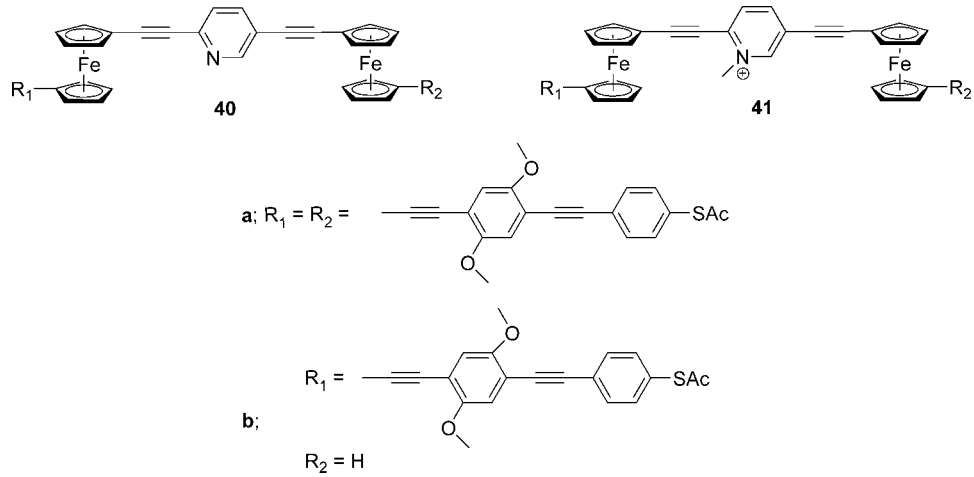

Figure 26. Structure of complexes **40** and **41** (**a** and **b** for both).

Table 20. Electrochemical Data for the Family of Complexes 40 and 41[a]

complex	E_1 (V)	E_2 (V)	ΔE (mV)
40a[b]	+0.94		0
40b[b]	+0.86	+0.99	130
41a[b]	+1.04	+1.23	190
41b[b]	+0.95	+1.26	310

[a] All redox potentials are relative to $[Cp^*_2Fe]^+/Cp^*_2Fe$. [b] Data from ref 183.

whereas the ferrocene on the right-hand side is only *meta*-conjugated with the pyridinium cation.

4. Systems with Aromatic Rings as Bridges

4.1. Fulvalene and Fulvalene-like Bridged Systems

Fulvalene consists of two Cp units attached by a double bond and is highly unstable with respect to dimerization and polymerization. Figure 27 represents the different type of fulvalene ligands. It can be doubly reduced to form the fulvalene dianion, also known as bicyclopentadienyl (I) or fulvalendiyl (Fv). The fulvalene bridge can also contain substituted cyclopentadienes (substituted fulvalene), leading to asymmetric ligands, such as Cp-indenyl (II). They have been extensively used as ligands to form bimetallic complexes and possess a notable efficiency in promoting interactions between the metal centers.[22] Fulvalene-like bridges correspond to species that present two aromatic rings linked directly such as two phenyl rings (III). These types of systems, including both homo- and heterobimetallic complexes, have been extensively reviewed by different authors until 2004.[20,22,184–186]

Bimetallic Fv complexes exhibit very particular properties relative to their monometallic analogues as the π-system of the Fv fragment enhances the electronic interactions of the metal centers through the ligand. This occurs regardless of the geometry of the metal centers (cisoid or transoid) with respect to the Fv ligand and of the existence of metal−metal bonds. Complexes with Fv ligands are generally resistant to fragmentation and maintain the two metal centers in close proximity.[187] Figure 27 also represents the cisoid and transoid geometries observed in bimetallic Fv complexes.

Many of the compounds that have been reported and studied using fulvalene, substituted fulvalene and fulvalene-like bridges as ligands are heterobimetallic. [η^6-(2-Ferrocenyl)indene]-$Cr(CO)_3$, [η^6-(3-ferrocenyl)indene]-$Cr(CO)_3$, [η^5-(1-ferrocenyl)indenyl]-RhL_2 (L = COD), and [η^5-(2-ferrocenyl)indenyl]-RhL_2 (L = CO) have been classified as class II systems,[5] while [η^5-(2-ferrocenyl)indenyl]-RhL_2 (L = COD, nbd) have been ascribed to borderline class II/class III systems (where COD = 1,5-cyclooctadiene and nbd = norbornadiene).[25] The quasi-symmetric and almost planar η^5-(2-ferrocenyl)indenyl bridging ligand and the Rh coordinated olefins COD and nbd, both contribute to ensure a more efficient electron-transfer from Rh to Fe centers.

$[Cp^*Ti(\mu\text{-}Cl)]_2[\eta^5\text{:}\eta^5\text{-Fv}]$[188] and $[P(CH_2NPh)_3Zr]_2[\eta^5\text{:}\eta^5\text{-Fv}]$[189] are homobimetallic complexes using Fv. Both species have been characterized by NMR spectroscopy and X-ray diffraction. Further studies have not been reported. [η^5-(2-ferrocenyl)indenyl]FeCp, previously synthesized in 1999,[190] have been recently further studied by Santi and Ceccon.[191] Electrochemical data (ΔE = 370 mV and $K_c = 2.3 \times 10^6$) and UV−vis/NIR data ($\bar{\nu}_{max}$ = 6010 cm^{-1}, $\Delta\bar{\nu}_{1/2(calcd)}$ = 3560 cm^{-1}, $\Delta\bar{\nu}_{1/2(obs)}$ = 3020, and Γ = 0.4) have suggested that this complex correspond to a class II system.

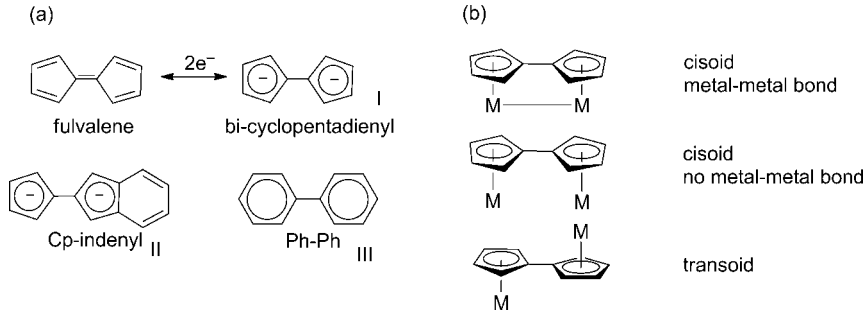

Figure 27. (a) Fv ligands and (b) cisoid and transoid geometry with or without a metal−metal bond.

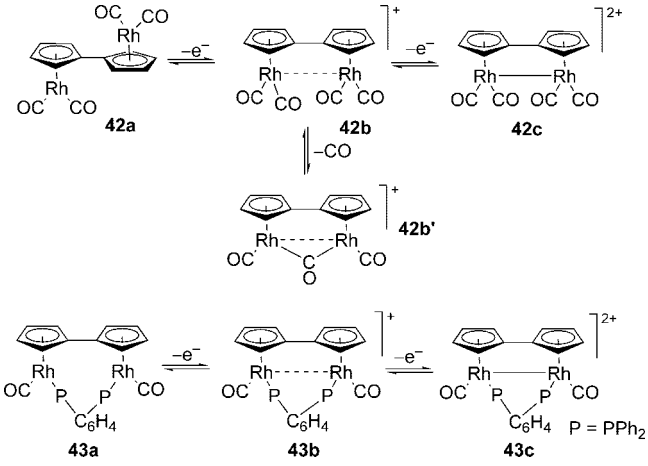

Figure 28. Summary of oxidation processes for **42a** and **43a** proposed by Geiger et al.[192]

Table 21. IR Frequencies for Complexes 42a−c, 42b′ and 43a−c[a]

complex	IR (cm^{-1}) ν_{CO}	
42a[b]	1978	2038
42b[b]	2070	2105
42b[b]	1881	2073
42c[b]	2123	2153
43a[b]	1942	
43b[b]	1992	2024
43c[b]	2054	2082

[a] IR data measured in CH_2Cl_2. [b] Data from ref 192.

Geiger et al.[192] have performed electrochemical studies on (Fv)dirhodium systems, where they manipulated the conditions to favor either one- or two-electron oxidation processes. As mentioned in the theoretical aspects (section 2), if two one-electron processes are observed, the ΔE value corresponds to the difference $E_2 - E_1$. For most complexes, ΔE has a positive value, therefore the mixed-valence complex is thermodynamically stable. In limited cases, ΔE presents a negative value, where the normal ordering of E_1 and E_2 is "inversed". A single two-electron wave can then be observed and the mixed-valence system exists only in low equilibrium concentrations. A number of factors are known to affect ΔE values, such as the solvent and electrolyte.[192] Geiger et al.[193] have synthesized $FvRh_2(CO)_4$ (**42a**) and $FvRh_2(CO)_2(\mu$-dppm) (**43a**, where dppm = bis-diphenylphosphinomethane)) in 1996. These systems exhibit single two-electron oxidations using $[NBu_4]^+[PF_6]^-$ as an electrolyte. In both complexes, the mixed-valence species are not detected. If CV is performed in less ion-pairing media (weakly coordinating anions), such as $[B(C_6H_5)_4]^-$, positive values of ΔE are observed (125 mV for **42a−c** and 90 mV for **43a−c**) and the mixed-valence species could be synthesized in the time scale of the CV studies. They have been characterized by in situ IR spectroscopy. The analyses of the shifts of the ν_{CO} bands in the neutral and cationic species indicate the existence of an electronic coupling between the metal centers, which also supports the formation of metal−metal bonds in both mixed-valence systems.

Figure 28 represents the expected structure of the mixed-valence complexes **42b** and **43b**. Table 21 displays IR carbonyl stretchings for **42a−c**, **42b′**, and **43a−c**. Complex **42b′** is most likely formed by the loss of CO of **42b**.[192] To summarize, both electrochemical and IR studies support the existence of metal−metal interactions in both di-Rh complexes.

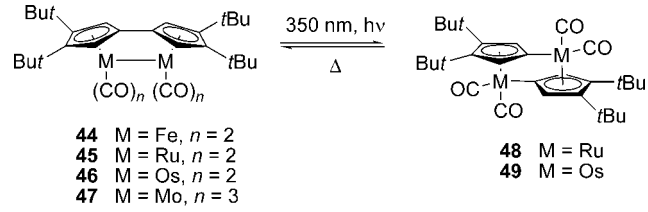

44 M = Fe, *n* = 2
45 M = Ru, *n* = 2
46 M = Os, *n* = 2
47 M = Mo, *n* = 3

48 M = Ru
49 M = Os

Figure 29. Structures of complexes **44−47** and photogeneration of **48** and **49**.

To stabilize the fulvalene fragment, substituents can be added to sterically protect it from dimerization. For example, 2,2′,3,3′-tetra-*tert*-butylfulvalene has been used to synthesize some complexes **44−47**.[194] These highly stable systems have been studied by NMR, IR, and X-ray diffraction. Irradiation of **44−46** yields the isomers **48** and **49**, from **45** and **46**, respectively. Complex **44** is inert under the investigated conditions. Complex **45** can be quantitatively retrieved when heating **48** at 75 °C for 5 h, whereas **49** is completely stable under these conditions. Figure 29 shows complexes **44−47** and the synthesis of **48** and **49** from **45** and **46**, respectively. Studies on metal−metal interactions have not been carried out.

The fulvalene-like bridged ligand Cp-CR_2-indene has been used to synthesize a family of complexes containing two Ru centers (Figure 30, **50a−g**).[195] They have been characterized by NMR spectroscopy and X-ray diffraction but metal−metal interactions studies have not yet been achieved. This example has been included, even though the bridge is not conjugated, to give an insight of recently synthesized fulvalene-like bridged complexes.

Figure 30 shows the mixed-valence complex $[Cp^*Ru(\mu\text{-}\eta^6{:}\eta^2\text{-ptpy})RuCp^*Cl_2]_2[Hg_2Cl_6]$ (**51**, Hptpy = 2-(4-tolyl)-pyridine), which contains a Cp^*Ru^{II} and a $[Cp^*Cl_2Ru^{IV}(ptpy)]^+$ fragment. It has been characterized by NMR spectroscopy and X-ray diffraction.[196] The Ru^{II} moiety has a sandwich structure, whereas the Ru^{IV} possesses a four-legged piano-stool. The fulvalene-like bridged ligand is not coplanar. The Cp*(Ct)−Ru^{IV} distance is longer than the Cp*(Ct)−Ru^{II} (1.912 and 1.717 Å, respectively), which could mean that the system is valence trapped in the time scale of the experiment (Ct = centroid). However, it is important to consider the different environment of both Ru centers and the high asymmetry of the molecule.

4.2. Fused Delocalized Polycyclic Bridged Systems

Metal−metal interactions can be significant when metal centers are connected through a common π-system, such as conjugated, fused-ring polycyclic hydrocarbon bridges. They form a rigid molecular backbone structure, which allows and controls electronic delocalization. Homobimetallic complexes are more commonly synthesized. Incorporating different metal centers into the system is difficult, as the ligands used in most reactions are in their dianionic forms.

In this section, complexes with fused polycyclic bridges, such as indenyl anion (Ind, **52**), pentalene-diide (Pn, **53**), permethylpentalene-diide (Pn*, **54**), naphthalene-diide (**55**), *s*-indacene-diide (**56**), *as*-indacene-diide (**57**), and permethylfluorene (Flu*H, **58**) are presented, emphasizing their delocalization and intramolecular metal-to-metal communication properties. Figure 31 illustrates the fused delocalized polycyclic ligands. They are most commonly reacted as

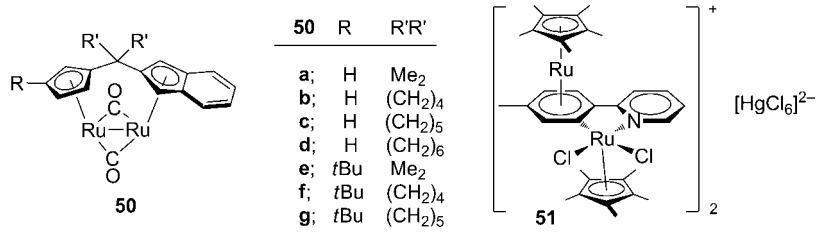

Figure 30. Structures of complexes **50a−g** and **51**.

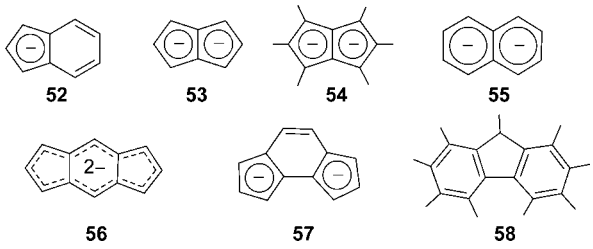

Figure 31. Fused polycyclic bridges utilized as ligands **52−58**.

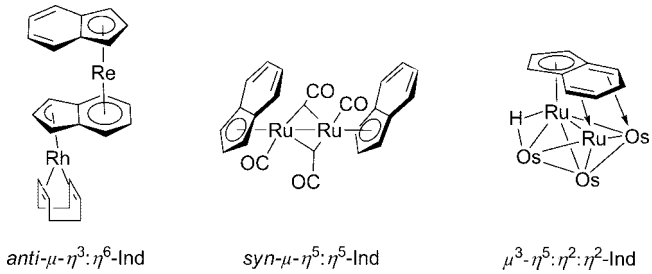

Figure 32. Examples of diverse coordination modes that the Ind fragment can adopt.

anionic salts, although Flu*H has only been used in its neutral form to yield bimetallic complexes.

4.2.1. Indene, Pentalene, Permethylpentalene, and Naphthalene

Indenyl (Ind) bridged systems have received a great deal of attention due to the diverse and flexible hapticities the Ind fragment can adopt. Examples are *anti*-μ-η^3:η^6-Ind,[197] *syn*-μ-η^5:η^5-Ind[198] and μ^3-η^5:η^2:η^2-Ind[199] coordination modes (Figure 32). Ind is an aromatic ten π-electron system. Only a few examples of bridged bis(Ind) dinuclear metal complexes have been reported,[200–204] mainly because of the poor reactivity of the Ind ligands.[205]

Figure 33a displays the structure of the slipped μ-Ind triple-decker complexes of dicobalt (**59**) and diruthenium (**60a−c**).[206,207] The di-Ru systems present interesting redox behaviors. Each of the complexes (**60a−c**) undergoes an irreversible oxidation and a quasi-reversible reduction. Kudinov et al.[206,207] have suggested that each event is a two-electron process and that oxidation and reduction occur at the η^5:η^5- and η^5:η^6-centers, respectively. However, the two metal centers are in different chemical environments in each complex, which could affect electrochemical behavior of the Ru centers. It has been determined that the two-electron reduction occurred at the metal center coordinated to the six-membered ring as it has a more positive charge. Consequently, the Ru atom coordinated to the five-membered ring experienced a two-electron oxidation. The oxidized metal (Ru^{IV}) could be stabilized by the coordination of a solvent molecule (Solv), as it has been observed for mononuclear Ind complexes.[208] This is supported by comparing the electrochemical behavior of ruthenocene (oxidation at +0.80 V relative to SCE)[209] and $[CpRu(C_6H_6)]^+$ (reduction at −2.02 V relative to SCE) (Figure 33 (b)).[210] The di-Co compound **59** presents a complicated redox behavior with one irreversible oxidation (−0.09 V), assigned to a decomposition product and a quasi-reversible process at a higher potential (+0.22 V). The latter process is more likely to be because of the solvated MeCN complex [Cb*Co(μ-η^5:η^4-Ind)Co(MeCN)Cb*]$^+$ (where Cb* = 1,2,3,4-tetramethylcyclobutadiene).[206] These studies suggest that in all these complexes, the metals do not display a significant electronic communication through the Ind bridge.

Wang et al.[205] have studied the synthesis and structures of silyl bridged bis(Ind) diruthenium complexes. The general reaction path to incorporate $Ru_3(CO)_{12}$ into an indene bridge is to heat the indene ligand and $Ru_3(CO)_{12}$ in a refluxing high boiling point alkane, such as heptane. When the same

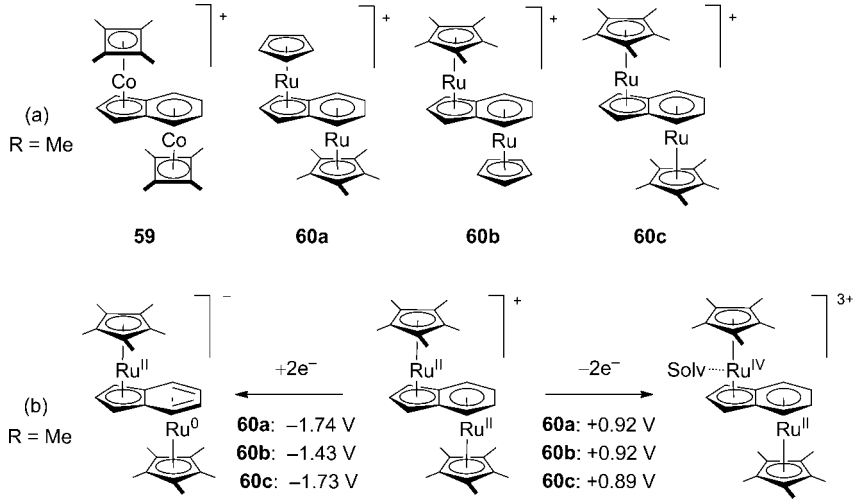

Figure 33. (a) Di-Co (**59**) and di-Ru (**60a−c**) Ind complexes and (b) redox behavior of complexes **60a−c**.[206,207] All redox potentials are relative to SCE.

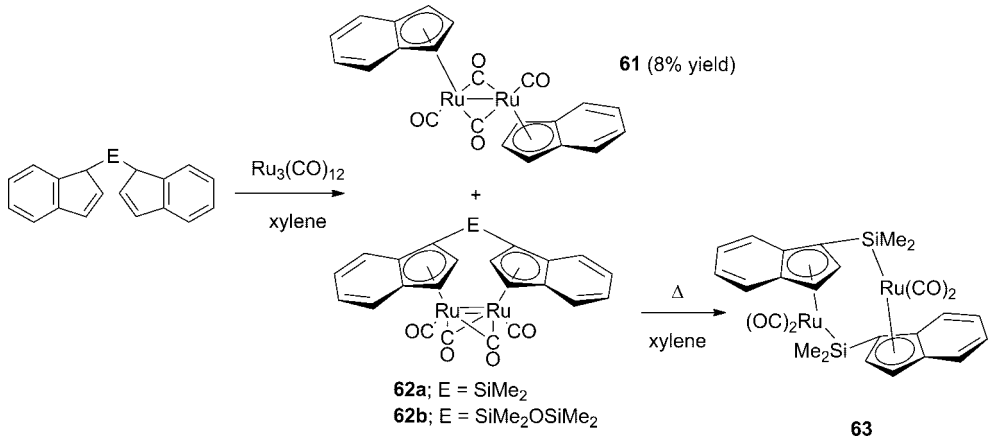

Figure 34. Silyl bridged bis(Ind) di-Ru complexes **61**, **62a** and **b**, and **63**.

procedure with the silyl-bridged bis(indene) ligand was used, only the desilylation product $[\eta^5\text{-IndRu(CO)}(\mu\text{-CO})]_2$ is formed (**61**). However, the replacement of the alkane solvent by xylene yields the expected silylated di-Ru complex (**62a** and **b**) as main products. Complex **62a** can be converted to **63** upon heating (~140 °C) where a thermal rearrangement occurs. Figure 34 shows the synthesis of complexes **61**−**63**.

If the same reaction is pursued using a nonbridged substituted indene as a ligand, a complex analogous to **61** is formed.[211] All these complexes have been characterized and studied by NMR and IR spectroscopy, and their structures have been confirmed by X-ray diffraction. However, studies on their electronic properties have not been reported.

The pentalene dianion (Pn, $C_8H_6^{2-}$) is a ten π-electron aromatic system that can be regarded as two Cp rings sharing an edge; salts of the dianion are stable in inert atmosphere. The neutral unsubstituted form C_8H_6 is thermally unstable and dimerizes at low temperatures (−196 °C). 1,5-Dihydropentalene (PnH_2) is found to be thermally unstable at room temperature, but may be stored under an inert atmosphere at −20 °C, with traces amount of hydroquinone, without degradation.[212] Summerscales and Cloke[213] have extensively reviewed the organometallic chemistry of Pn and its properties. The degree of electronic delocalization in the mixed-valence forms of these systems is one of the largest known for fused polycyclic-bridged organometallic complexes.[214] *anti*-$[(CO)_3Mn]_2(\mu\text{-}\eta^5\text{:}\eta^5\text{-Pn})$ displays a ΔE value of 410 mV meaning that both $Mn(CO)_3$ fragments are not behaving like two separate units. Its mono-anion, formally a Mn^I/Mn^0 mixed-valence complex, has been ascribed as at least a borderline class II/class III or a class III system due to the hyperfine coupling of the two equivalent Mn^{55} ($I = 5/2$) centers in the EPR (X-band) spectrum. Also, in the UV−vis/NIR, the bandwidth at half height observed ($\Delta\bar{\nu}_{1/2(obs)} = 2810$ cm^{-1}) is narrower than the bandwidth at half height calculated ($\Delta\bar{\nu}_{1/2(calcd)} = 5440$ cm^{-1}) and the energy of this transition is independent of the polarity of the solvent.[82] The family of complexes $[(Cp^*M)_2Pn]^{n+}$ (M = Fe, Co, Ni; n = 0, 1, 2) displays delocalized strong electron coupling between metal sites. This results in large ΔE values (850 mV for Fe, 710 mV for Co, 650 mV for Ni, and 290 mV for Ru) and varying degrees of intramolecular coupling between metal centers containing unpaired spins. Their mixed-valence analogues ($n = +1$) have ICT absorption bands that are independent of the polarity of the solvent and that are not observed for the neutral ($n = 0$) or the dicationic species ($n = +2$). These absorption bands exhibit widths at half height

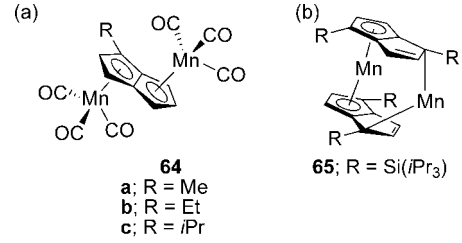

Figure 35. Substituted di-Mn systems: (a) 1-alkylpentalenyl **64a**−**c** and (b) 1,4-silylpentalenyl **65**.

Table 22. Electrochemical Data for 64a−c and Unsubstituted *anti*-$[(CO)_3Mn]_2(\mu\text{-}\eta^5\text{:}\eta^5\text{-Pn})$[a]

complex	E_1 (V)	E_2 (V)
64a[b]	−1.93	−2.35
64b[b]	−1.90	−2.37
64c[b]	−1.90	−2.36
anti-$[(CO)_3Mn]_2(\mu,\eta^5\text{:}\eta^5\text{-Pn})$[b]	−1.91	−2.32

[a] All redox potentials are relative to $[Cp_2Fe]^+/Cp_2Fe$. [b] Data from ref 214.

($\Delta\bar{\nu}_{1/2(obs)}$) that are significantly narrower than the calculated one ($\Delta\bar{\nu}_{1/2(calcd)}$).[83]

Polynuclear Pn complexes are characterized by their low solubility, which makes their synthesis and characterization very difficult. However, as observed for Cp and Cp*, the addition of methyl groups to the carbon framework can enhance the solubility of the systems. Figure 35a illustrates the structure of the 1-alkylpentalenyl dimanganese complexes *anti*-$[(CO)_3Mn]_2(\mu\text{-}\eta^5\text{:}\eta^5\text{-Pn}^{1-R})$ (**64a**−**c**). These systems display greater solubility relative to their unsubstituted analogues.[214]

CV studies show two quasi-reversible reductions for **64a**−**c** at very similar redox potentials. They are also very similar to the ones found for the unsubstituted species (Table 22).[214] This demonstrates that the alkyl group does not have a great effect on the metal−metal interactions.

Cloke et al.[215] have used a doubly substituted Pn ligand to synthesize the interesting complex $[1,4\text{-Si}(i\text{Pr}_3)\text{-Pn}]_2Mn_2$ (**65**, Figure 35b). Magnetic data, X-ray diffraction, and DFT calculations suggest that the system presents two weakly interacting metal centers (suggested by the calculated fractional Mn−Mn bond order of 0.60), one in a HS and the other in LS configuration, in different coordination environments. The HS Mn center shows a low coordination number ($\eta^1\text{:}\eta^1$), whereas the LS displays typical metallocene coordination ($\eta^5\text{:}\eta^5$). The di-Cr analogue, which has also been synthesized and studied by Cloke et al.,[216] exhibits an η^5:

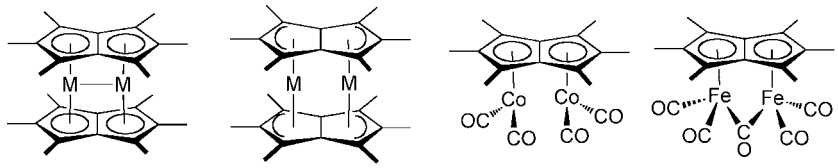

66; M = V
67; M = Cr
68; M = Mn
69; M = Co

70; M = Ni

71

72

Figure 36. Family of fused double metallocene complexes **66**−**70** and half-sandwich metal carbonyl complexes **71** and **72**.

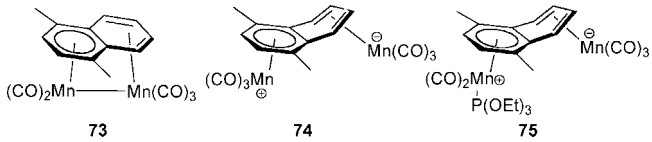

73 **74** **75**

Figure 37. Di-Mn η^4:η^6-naphthalene complexes **73**−**75**.

η^5-coordination for both metal centers. Furthermore, structural data reveals a metal−metal bond (Cr═Cr), indicating a strong electronic interaction between them.

Recently, O'Hare et al.[217,218] have developed the synthesis of the permethylated analogue of Pn, referred to as Pn*. The organometallic complexes that have been synthesized with this ligand show enhanced solubility and stability properties compare to their nonalkylated analogues. Fused double metallocenes of the type $Pn^*_2M_2$ (where M = V **66**, Cr **67**, Mn **68**, Co **69**, and Ni **70**) present η^5:η^5 coordination and metal−metal bonds. However, when M = Ni, the coordination is effectively η^3:η^3 and a metal−metal bond is not present. Clearly, the system is able to adapt to each metal center to stabilize the compound, displaying different coordination modes.[212,219,220] Half-sandwich complexes *syn*-$Pn^*M_2(CO)_n$ (M = Co, n = 4, **71**; M = Fe, n = 5, **72**) have been prepared and studied.[221] Structural data and DFT calculations reveal the absence of metal−metal bonds. Different studies in these types of complexes are ongoing to determine the extent of the interactions between the metal centers. Figure 36 shows the family of Pn* complexes **66**−**72**.

Arene ligands presenting metals bound in a η^6-configuration are another important class of organometallic complexes. Sweigart et al.[222] have synthesized and studied *syn*-facial bimetallic η^4:η^6-naphthalene complexes. (η^4:η^6-1,4-Me_2naphthalene)$Mn_2(CO)_5$ (**73**) can be reversibly converted into the zwitterionic (η^4:η^6-1,4-Me_2naphthalene)$Mn_2(CO)_6$ (**74**), with a CO atmosphere and ferrocenium. If the same reaction is performed in the presence of $P(OEt)_3$, (η^4:η^6-1,4-Me_2naphthalene)$Mn_2(CO)_5P(OEt)_3$ (**75**) is obtained. Figure 37 depicts the di-Mn η^4:η^6-naphthalene complexes **73**−**75**. X-ray diffraction reveals the proximity of both metal centers in **74** and **75**, both systems having a 45° bend of the naphthalene ring and cleavage of the Mn−Mn bond. IR spectroscopy indicates a large charge separation in system **74**, having two different sets of bands for both η^4- and η^6-bonded $Mn(CO)_3$ fragments at 1980 and 1880 cm^{-1} and 2050 and 1980 cm^{-1}, respectively.

4.2.2. s-Indacene, as-Indacene, and Permethylfluorene

The indacene dianion is a fourteen π-electron aromatic ligand. It can be in two isomeric forms: *s*- or *as*-. Many homo- and heterobimetallic complexes with these two ligands have been synthesized and studied with respect to their metal−metal interactions.[20] Chavez et al.[2] have prepared and studied the properties of *syn*- and *anti*-isomers (**76**) (Figure

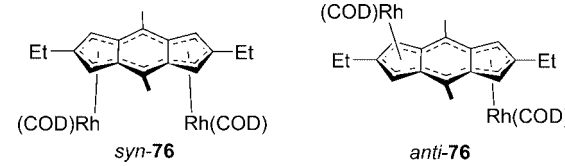

syn-**76** *anti*-**76**

Figure 38. *syn*- and *anti*-Isomers of (2,6-diethyl-4,8-dimethyl-*s*-indacene)$[Rh(COD)]_2$ (**76**).

Table 23. Electrochemical and Catalytic Data for Mono- and Bimetallic *s*-Indacene-Rh Complexes

complex	E_a (V)	$E_a - E_c$ (mV)	time[a] (min)
(2,6-diethyl-4,8-dimethyl-*s*-indacene)[Rh(COD)][b]	+1.42	140	450
syn-**76**[b]	+0.37	90	180
anti-**76**[b]	+0.46	170	35

[a] Time = time in minutes when all the styrene has reacted. [b] Data from ref 2.

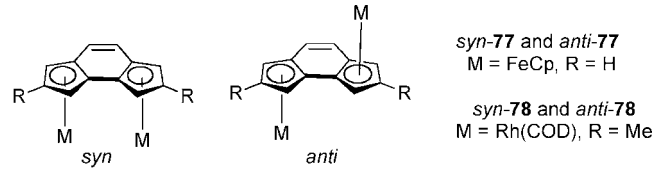

Figure 39. *syn*- and *anti*-Isomers of *as*-indacene di-Fe and di-Rh complexes **77** and **78**.

38) of (2,6-diethyl-4,8-dimethyl-*s*-indacene)$[Rh(COD)]_2$ and compared their properties with its monometallic analogue (2,6-diethyl-4,8-dimethyl-*s*-indacene)[Rh(COD)].

CV and catalytic studies for the hydrogenative silylation of styrene suggest that both isomers exhibit metal−metal interactions. Higher catalytic activity can be attributed to strong electronic interactions.[2] However, *syn*-**76** displays steric hindrance because of the proximity of the two Rh centers. The ligand loses its aromaticity due to a slight displacement from planarity, which was confirmed by X-ray diffraction. Consequently, the electronic communication is affected. Table 23 summarizes the electrochemical and catalytic data for **76** and (2,6-diethyl-4,8-dimethyl-*s*-indacene)-[Rh(COD)]. *syn*-**76** exhibits an irreversible one-electron electrochemical process and a low activity as a catalyst relative to *anti*-**76**, which displays a quasi-reversible one-electron electrochemical process and a higher activity. The monometallic analogue also presents a one-electron process at more positive potentials and a longer reaction time compared to the bimetallic systems.

Figure 39 displays the *syn*- and *anti*-isomers of (*as*-indacene)$[FeCp]_2$ (**77**) and (*as*-dimethylindacene)$[Rh(COD)]_2$ (**78**). Metal−metal interactions have been studied by CV and UV−vis/NIR spectroscopy.[24,223]

Table 24 summarizes their electrochemical and UV−vis/NIR data. *syn*-**77** and *anti*-**77** display reversible two one-electron waves with comparable ΔE values (640 and 631

Table 24. Electrochemical and UV−vis/NIR Data for the Family of Complexes 77 and 78[a]

	CV data				UV−vis/NIR data for MV species				
complex	E_1 (V)	E_2 (V)	ΔE (mV)	K_c	$\bar{\nu}_{max}$ (cm^{-1})	H_{ab} (cm^{-1})	$\Delta\bar{\nu}_{1/2(obs)}$ (cm^{-1})	$\Delta\bar{\nu}_{1/2(calcd)}$ (cm^{-1})	Γ
syn-**77**[b]	+0.12	+0.76	640	9.3×10^{10}	7170 (395[c])	460	3590	3740	0.04
anti-**77**[b]	+0.10	+0.73	630	7.0×10^{10}	5025 (765[c])	430	2860	3130	0.09
syn-**78**[b]	+0.09	+0.42	330	4.4×10^{5}	8660 (2070[c])	4330[d]	1830	4110	0.56
anti-**78**[b]	+0.26	+0.65	390	5.1×10^{6}	6485 (5175[c])	3240[d]	1350	3560	0.62

[a] All redox potentials are relative to SCE. [b] Data from ref 24. [c] ε, in M^{-1} cm^{-1}. [d] Calculated with expression $H_{ab} = \bar{\nu}_{max}/2$.

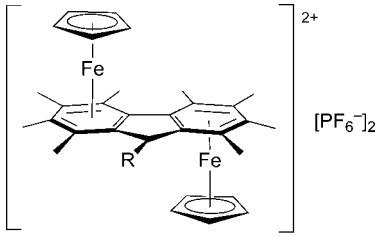

79
a; R = H
b; R = Me

Figure 40. Bimetallic Fe complexes of Flu*H (**79a**) and Flu″H (**79b**).

mV respectively) indicating that the thermodynamic stability of the mixed-valence complexes are similar ($K_c \approx 10^{11}$). Oxidation of *anti*-**78** occurs at a more positive potential (+0.26 V) compared to *syn*-**78** (+0.09 V). These two systems present lower thermodynamic stability than their Fe analogues, with K_c values of 10^6 and 10^5 for *anti*-**78** and *syn*-**78**. They also show lower ΔE values of 390 and 328 mV, respectively.

The mixed-valence cations of all these species display characteristic ICT bands by UV−vis/NIR spectroscopy. *syn*-**77**$^+$ and *anti*-**77**$^+$ correspond to localized class II systems with Γ values of 0.04 and 0.09, respectively (weakly coupled class II $0 < \Gamma < 0.1$). *syn*-**78**$^+$ and *anti*-**78**$^+$ exhibit Γ values of 0.56 and 0.62 respectively, corresponding to a borderline class II/class III system ($\Gamma \approx 0.5$) and a delocalized class III complex ($\Gamma > 0.5$), respectively. Overall, despite the proximity of the two metal centers in *syn*-isomers, the electronic communication occurs mostly through the ligand rather than through space.

Organometallic complexes containing fluorene (FluH) and fluorenyl (Flu) ligands have been extensively studied because of the interesting qualities of the Flu fragment.[224,225] The deprotonated fluorenyl can be considered as a Cp fragment fused to two benzene groups, and can form monometallic complexes with a variety of coordination modes, such as η^1, η^3, and η^5.[226,227] FluH can also be viewed as a CH_2-bridged biphenyl unit with two potential binding sites on the arene rings (η^5 and η^6 configurations). Considering these properties and the striking differences observed when alkylated analogues of Cp and Pn are used, the nonamethylated fluorene analogue (Flu*H) have been synthesized.[228] Neutral Flu*H and octamethylfluorene (Flu"H) ligands have been used to obtain the complexes $[(CpFe)_2Flu*H]^{2+}[PF_6^-]_2$ (**79a**) and $[(CpFe)_2Flu"H]^{2+}[PF_6^-]_2$ (**79b**).[229] These two compounds have been characterized by NMR spectroscopy and X-ray diffraction (only **79b**), demonstrating that each Fe possesses a η^6-binding mode to each arene fragment. Figure 40 depicts the structure of complexes **79a** and **b**.

Table 25 shows the electrochemical data for **79a**, **b**, $[(CpFe)_2FluH]^{2+}[PF_6^-]_2$, and $[(Cp*Fe)_2FluH]^{2+}[PF_6^-]_2$. The cyclic voltammogram exhibits a cascade of four redox waves for **79a** and **b**. The first two (E_1 and E_2) correspond to

Table 25. Electrochemical Data for Bimetallic Fe Complexes of FluH, Flu*H, and Flu″H[a]

complex	E_1 (V)	E_2 (V)	ΔE (mV)
$[(CpFe)_2FluH]^{2+}[PF_6^-]_2$[b,d]	−1.14	−1.32	180
$[(Cp*Fe)_2FluH]^{2+}[PF_6^-]_2$[b,d]	−1.39	−1.69	300
79a[c,d]	−1.26	−1.61	350
79b[c,d]	−1.26	−1.65	390

[a] Only the first two redox events shown. All couples are relative to $[Cp_2Fe]^+/Cp_2Fe$. [b] Measured in DMF. [c] Measured in MeCN. [d] Data from ref 228.

stepwise one-electron reversible reductions of the Fe centers ($Fe^{II}Fe^{II} \rightarrow Fe^{II}Fe^{I} \rightarrow Fe^{I}Fe^{I}$). The third process is irreversible because of the rearrangement of the ligand after reduction. The fourth appears to be a two-electron irreversible wave. Both systems display very similar electrochemical behavior meaning that the extra methyl group of Flu*H compared to Flu″H does not greatly affect the properties of the system. These compounds are reduced at more negative potential than their nonmethylated analogues $[(CpFe)_2FluH]^{2+}[PF_6^-]_2$ and $[(Cp*Fe)_2FluH]^{2+}[PF_6^-]_2$, as a result of the increased electron donation from the methyl groups on the Flu*H and Flu″H ligands. This means that the mixed-valence complexes are more stabilized as methylated species **79a**$^+$ and **b**$^+$, and the existence of metal−metal interactions in all the complexes. This is as expected; the increased inductive effects of the methyl groups act to enhance the electron exchange interaction.[230] This can be supported by the ΔE values: 180 mV (in DMF) for $[(CpFe)_2FluH]^{2+}[PF_6^-]_2$, 300 mV (in DMF) for $[(Cp*Fe)_2FluH]^{2+}[PF_6^-]_2$, 350 mV (in MeCN) for **79a**, and 390 mV (in MeCN) for **79b**.

5. Summary

Metal−metal interactions have been studied in a large number of different carbon bridged homobinuclear complexes. The bridging ligands considered are sp^2- and/or sp-hydrocarbon chains, bridging aromatic rings linked directly as fulvalene and fulvalene-like; and fused aromatic spacers as indenyl, permethylpentalene-diide, and permethylfluorene between others. The efficiency of the intramolecular electronic communication between the metal centers depends on the nature of the metals, their oxidation state, the strength of the coupling between the acceptor and the donor sites, the ancillary ligands and the structure of the bridging ligand.

Generally, the electronic communication decreases with increasing the distance between the donor and the acceptor sites. Also, electronic coupling and other donor−acceptor interactions are stronger through alkene than alkyne bridges. Bridging aromatic rings and fused aromatic linkers are also suitable spacers to promote metal−metal interactions. However, if their planarity is broken due to steric effects, the loss of aromaticity decreases the electronic communication between the metal centers.

Metal−metal interactions have been mainly evaluated on the basis of IR, EPR, optical, and electrochemical measure-

ments of the mixed-valence species. According to these data, the numerous complexes presented on this review have been categorized following the Robin and Day classification.

6. Acknowledgments

We thank Dr. Steven Barlow for his insightful advice regarding this paper.

7. References

(1) Bencini, A.; Ciofini, I.; Daul, C. A.; Ferretti, A. *J. Am. Chem. Soc.* **1999**, *121*, 11418.
(2) Esponda, E.; Adams, C.; Burgos, F.; Chavez, I.; Manriquez, J. M.; Delpech, F.; Castel, A.; Gornitzka, H.; Riviere-Baudet, M.; Riviere, P. *J. Organomet. Chem.* **2006**, *691*, 3011.
(3) Ferretti, A.; Lami, A.; Villani, G. *J. Phys. Chem. A* **1997**, *101*, 9439.
(4) Long, N. J. *Angew. Chem., Int. Ed. Engl.* **1995**, *34*, 21.
(5) Santi, S.; Ceccon, A.; Bisello, A.; Durante, C.; Ganis, P.; Orian, L.; Benetollo, F.; Crociani, L. *Organometallics* **2005**, *24*, 4691.
(6) Santi, S.; Orian, L.; Donoli, A.; Durante, C.; Bisello, A.; Ganis, P.; Ceccon, A. *Organometallics* **2007**, *26*, 5867.
(7) Ward, M. D. *Chem. Soc. Rev.* **1995**, *24*, 121.
(8) Balzani, V.; Juris, A.; Venturi, M.; Campagna, S.; Serroni, S. *Chem. Rev.* **1996**, *96*, 759.
(9) Belser, P.; Bernhard, S.; Blum, C.; Beyeler, A.; De Cola, L.; Balzani, V. *Coord. Chem. Rev.* **1999**, *192*, 155.
(10) De Cola, L.; Belser, P. *Coord. Chem. Rev.* **1998**, *177*, 301.
(11) Low, P. J.; Roberts, R. L.; Cordiner, R. L.; Hartl, F. *J. Solid State Electrochem.* **2005**, *9*, 717.
(12) Newton, M. D. *Chem. Rev.* **1991**, *91*, 767.
(13) Paul, F.; Lapinte, C. *Coord. Chem. Rev.* **1998**, *178*, 431.
(14) Sarkar, B.; Laye, R. H.; Mondal, B.; Chakraborty, S.; Paul, R. L.; Jeffery, J. C.; Puranik, V. G.; Ward, M. D.; Lahiri, G. K. *J. Chem. Soc., Dalton Trans.* **2002**, 2097.
(15) Kim, B.; Beebe, J. M.; Olivier, C.; Rigaut, S.; Touchard, D.; Kushmerick, J. G.; Zhu, X. Y.; Frisbie, C. D. *J. Phys. Chem. C* **2007**, *111*, 7521.
(16) Kaim, W.; Lahiri, G. K. *Angew. Chem., Int. Ed.* **2007**, *46*, 1778.
(17) Kowalski, K.; Linseis, M.; Winter, R. F.; Zabel, M.; Zalis, S.; Kelm, H.; Kruger, H. J.; Sarkar, B.; Kaim, W. *Organometallics* **2009**, *28*, 4196.
(18) Szesni, N.; Drexler, M.; Maurer, J.; Winter, R. F.; de Montigny, F.; Lapinte, C.; Steffens, S.; Heck, J.; Weibert, B.; Fischer, H. *Organometallics* **2006**, *25*, 5774.
(19) Adams, H.; Costa, P. J.; Newell, M.; Vickers, S. J.; Ward, M. D.; Felix, V.; Thomas, J. A. *Inorg. Chem.* **2008**, *47*, 11633.
(20) Ceccon, A.; Santi, S.; Orian, L.; Bisello, A. *Coord. Chem. Rev.* **2004**, *248*, 683.
(21) Delville, M. H. *Inorg. Chim. Acta* **1999**, *291*, 1.
(22) Barlow, S.; O'Hare, D. *Chem. Rev.* **1997**, *97*, 637.
(23) McCleverty, J. A.; Ward, M. D. *Acc. Chem. Res.* **1998**, *31*, 842.
(24) Santi, S.; Orian, L.; Durante, C.; Bencze, E. Z.; Bisello, A.; Donoli, A.; Ceccon, A.; Benetollo, F.; Crociani, L. *Chem.—Eur. J.* **2007**, *13*, 7933.
(25) Santi, S.; Orian, L.; Durante, C.; Bisello, A.; Benetollo, F.; Crociani, L.; Ganis, P.; Ceccon, A. *Chem.—Eur. J.* **2007**, *13*, 1955.
(26) Caballero, A.; Lloveras, V.; Curiel, D.; Tarraga, A.; Espinosa, A.; Garcia, R.; Vidal-Gancedo, J.; Rovira, C.; Wurst, K.; Molina, P.; Veciana, J. *Inorg. Chem.* **2007**, *46*, 825.
(27) Pastore, M.; Helal, W.; Isti, S. E.; Leininger, T.; Malrieu, J. P.; Maynau, D.; Angeli, C.; Cimiraglia, R. *J. Chem. Phys.* **2008**, 128.
(28) Ernst, S.; Kasack, V.; Kaim, W. *Inorg. Chem.* **2002**, *27*, 1146.
(29) Robin, M. B.; Day, P. *Adv. Inorg. Chem.* **1967**, *10*, 247.
(30) Marcus, R. A. *J. Chem. Phys.* **1956**, *24*, 966.
(31) Marcus, R. A. *Discuss. Faraday Soc* **1960**, 21.
(32) Marcus, R. A. *J. Chem. Phys.* **1965**, *43*, 679.
(33) Marcus, R. A. *J. Electroanal. Chem.* **1997**, *438*, 251.
(34) Brunschwig, B. S.; Creutz, C.; Sutin, N. *Chem. Soc. Rev.* **2002**, *31*, 168.
(35) Lancaster, K.; Odom, S. A.; Jones, S. C.; Thayumanavan, S.; Marder, S. R.; Bredas, J. L.; Coropceanu, V.; Barlow, S. *J. Am. Chem. Soc.* **2009**, *131*, 1717.
(36) Rehm, D. *Isr. J. Chem.* **1970**, *8*, 259.
(37) Closs, G. L.; Calcaterra, L. T.; Green, N. J.; Penfield, K. W.; Miller, J. R. *J. Phys. Chem.* **1986**, *90*, 3673.
(38) Anjan, C.; Debdeep, C.; Partha, H.; Debabrata, S.; Nilmoni, S. *Chem. Phys. Lett.* **2003**, *382*, 508.
(39) Chakraborty, A.; Chakrabarty, D.; Hazra, P.; Seth, D.; Sarkar, N. *Chem. Phys. Lett.* **2003**, *382*, 508.
(40) Kumbhakar, M.; Nath, S.; Mukherjee, T.; Pal, H. *J. Chem. Phys.* **2004**, *120*, 2824.
(41) Guldi, D. M.; Luo, C. P.; Prato, M.; Dietel, E.; Hirsch, A. *Chem. Commun.* **2000**, 373.
(42) Jiang, H.; Xu, H. J.; Ye, J. P. *J. Chem. Soc., Perkin Trans. 2* **2000**, *5*, 925.
(43) Zhang, J.; Unwin, P. R. *J. Chem. Soc., Perkin Trans. 2* **2001**, 1608.
(44) Diaz, C.; Arancibia, A. *Bol. Soc. Quim. Chilena* **1998**, *43*, 97.
(45) Guldi, D. M.; Asmus, K. D. *J. Am. Chem. Soc.* **1997**, *119*, 5744.
(46) Jayanthi, S. S.; Ramamurthy, P. *J. Phys. Chem. A* **1997**, *101*, 2016.
(47) Martini, I.; Hodak, J. H.; Hartland, G. V. *J. Phys. Chem. B* **1998**, *102*, 607.
(48) Sinha, S.; De, R.; Ganguly, T. *J. Phys. Chem. A* **1997**, *101*, 2852.
(49) Becker, H. G. O.; Pfeifer, D.; Urban, K. *J. Chem. Soc., Faraday Trans.* **1989**, *85*, 1765.
(50) Gould, I. R.; Ege, D.; Mattes, S. L.; Farid, S. *J. Am. Chem. Soc.* **1987**, *109*, 3794.
(51) Hill, R. H. *J. Chem. Soc., Chem. Commun.* **1989**, 293.
(52) Grampp, G. *Angew. Chem., Int. Ed. Engl.* **1993**, *32*, 691.
(53) Kapturkiewicz, A. *Chem. Phys.* **1992**, *166*, 259.
(54) Zagal, J. H.; Aguirre, M. J.; Vaschetto, M.; Retamal, B.; Pavez, J. *Bol. Soc. Quim. Chilena* **1994**, *39*, 43.
(55) Hush, N. S. *Prog. Inorg. Chem.* **1967**, *8*, 391.
(56) Hush, N. S. *Electrochim. Acta* **1968**, *13*, 1005.
(57) Hush, N. S. *Coord. Chem. Rev.* **1985**, *64*, 135.
(58) Coropceanu, V.; Andre, J. M.; Malagoli, M.; Bredas, J. L. *Theor. Chem. Acc.* **2003**, *110*, 59.
(59) Demadis, K. D.; Neyhart, G. A.; Kober, E. M.; White, P. S.; Meyer, T. J. *Inorg. Chem.* **1999**, *38*, 5948.
(60) Nelsen, S. F.; Trieber, D. A.; Ismagilov, R. F.; Teki, Y. *J. Am. Chem. Soc.* **2001**, *123*, 5684.
(61) Nelsen, S. F.; Ismagilov, R. F.; Trieber, D. A. *Science* **1997**, *278*, 846.
(62) Gao, L. B.; Liu, S. H.; Zhang, L. Y.; Shi, L. X.; Chen, Z. N. *Organometallics* **2006**, *25*, 506.
(63) Demadis, K. D.; Hartshorn, C. M.; Meyer, T. J. *Chem. Rev.* **2001**, *101*, 2655.
(64) Glover, S. D.; Goeltz, J. C.; Lear, B. J.; Kubiak, C. P. *Eur. J. Inorg. Chem.* **2009**, 585.
(65) LeVanda, C.; Bechgaard, K.; Cowan, D. O.; Mueller-Westerhoff, U. T.; Eilbracht, P.; Candela, G. A.; Collins, R. L. *J. Am. Chem. Soc.* **1976**, *98*, 3181.
(66) Westmoreland, T. D.; Wilcox, D. E.; Baldwin, M. J.; Mims, W. B.; Solomon, E. I. *J. Am. Chem. Soc.* **1989**, *111*, 6106.
(67) Morrison, W. H.; Hendrickson, D. N. *Inorg. Chem.* **1975**, *14*, 2331.
(68) Barlow, S.; Risko, C.; Chung, S. J.; Tucker, N. M.; Coropceanu, V.; Jones, S. C.; Levi, Z.; Bredas, J. L.; Marder, S. R. *J. Am. Chem. Soc.* **2005**, *127*, 16900.
(69) Gauthier, N.; Olivier, C.; Rigaut, S.; Touchard, D.; Roisnel, T.; Humphrey, M. G.; Paul, F. *Organometallics* **2008**, *27*, 1063.
(70) Piepho, S. B.; Krausz, E. R.; Schatz, P. N. *J. Am. Chem. Soc.* **1978**, *100*, 2996.
(71) Evans, C. E. B.; Naklicki, M. L.; Rezvani, A. R.; White, C. A.; Kondratiev, V. V.; Crutchley, R. J. *J. Am. Chem. Soc.* **1998**, *120*, 13096.
(72) Nelsen, S. F. *Chem.—Eur. J.* **2000**, *6*, 581.
(73) Creutz, C. *Prog. Inorg. Chem.* **1983**, *30*, 1.
(74) Fellows, E. A.; Keene, F. R. *J. Phys. Chem. B* **2007**, *111*, 6667.
(75) D'Alessandro, D. M.; Keene, F. R. *Pure Appl. Chem.* **2008**, *80*, 1.
(76) Kalyanasundaram, K.; Nazeeruddin, M. K. *Inorg. Chim. Acta* **1994**, *226*, 213.
(77) Barbara, P. F.; Meyer, T. J.; Ratner, M. A. *J. Phys. Chem.* **1996**, *100*, 13148.
(78) Launay, J. P. *Chem. Soc. Rev.* **2001**, *30*, 386.
(79) Kaim, W.; Klein, A.; Glockle, M. *Acc. Chem. Res.* **2000**, *33*, 755.
(80) Chen, P. Y.; Meyer, T. J. *Chem. Rev.* **1998**, *98*, 1439.
(81) D'Alessandro, D. M.; Keene, F. R. *Chem. Soc. Rev.* **2006**, *35*, 424.
(82) Jones, S. C.; Hascall, T.; Barlow, S.; O'Hare, D. *J. Am. Chem. Soc.* **2002**, *124*, 11610.
(83) Manriquez, J. M.; Ward, M. D.; Reiff, W. M.; Calabrese, J. C.; Jones, N. L.; Carroll, P. J.; Bunel, E. E.; Miller, J. S. *J. Am. Chem. Soc.* **1995**, *117*, 6182.
(84) Dembinski, R.; Bartik, T.; Bartik, B.; Jaeger, M.; Gladysz, J. A. *J. Am. Chem. Soc.* **2000**, *122*, 810.
(85) Goldsby, K. A.; Meyer, T. J. *Inorg. Chem.* **1984**, *23*, 3002.
(86) Hoshino, Y.; Suzuki, T.; Umeda, H. *Inorg. Chim. Acta* **1996**, *245*, 87.
(87) Sutton, J. E.; Sutton, P. M.; Taube, H. *Inorg. Chem.* **1979**, *18*, 1017.
(88) Sutton, J. E.; Taube, H. *Inorg. Chem.* **1981**, *20*, 3126.
(89) Barriere, F.; Camire, N.; Geiger, W. E.; Mueller-Westerhoff, U. T.; Sanders, R. *J. Am. Chem. Soc.* **2002**, *124*, 7262.
(90) Begley, M. J.; Mountford, P.; Stewart, P. J.; Swallow, D.; Wan, S. *J. Chem. Soc., Dalton Trans.* **1996**, 1323.

(91) Dickson, D. P. E.; Berry, F. J. *Mössbauer Spectroscopy*; Cambridge University Press: Cambridge, U.K., 1986.
(92) Kramer, J. A.; Hendrickson, D. N. *Inorg. Chem.* **1980**, *19*, 3330.
(93) McManis, G. E.; Nielson, R. M.; Weaver, M. J. *Inorg. Chem.* **1988**, *27*, 1827.
(94) Dong, T. Y.; Hendrickson, D. N.; Pierpont, C. G.; Moore, M. F. *J. Am. Chem. Soc.* **1986**, *108*, 963.
(95) Huang, W. L.; Schopfer, M.; Zhang, C.; Howell, R. C.; Gee, B. A.; Francesconi, L. C.; Polenova, T. *J. Phys. Chem. B* **2006**, *110*, 12340.
(96) Huang, W. L.; Schopfer, M.; Zhang, C.; Howell, R. C.; Todaro, L.; Gee, B. A.; Francesconi, L. C.; Polenova, T. *J. Am. Chem. Soc.* **2008**, *130*, 481.
(97) Lee, H.; Polenova, T.; Beer, R. H.; McDermott, A. E. *J. Am. Chem. Soc.* **1999**, *121*, 6884.
(98) Lee, Y. J.; Grey, C. P. *J. Phys. Chem. B* **2002**, *106*, 3576.
(99) Liu, K.; Ryan, D.; Nakanishi, K.; McDermott, A. *J. Am. Chem. Soc.* **1995**, *117*, 6897.
(100) Zhang, X. M.; Zhang, C.; Guo, H. Q.; Huang, W. L.; Polenova, T.; Francesconi, L. C.; Akins, D. L. *J. Phys. Chem. B* **2005**, *109*, 19156.
(101) Ooms, K.; Polenova, T.; Shough, A.-M.; Doren, D. J.; Nash, M. J.; Lobo, R. F. *J. Phys. Chem. C* **2009**, *113*, 10477.
(102) Daul, C.; Rauzy, C.; Decurtins, S.; Franz, P.; Hauser, A. *Int. J. Quantum Chem.* **2005**, *101*, 753.
(103) Kababya, S.; Nelson, J.; Calle, C.; Neese, F.; Goldfarb, D. *J. Am. Chem. Soc.* **2006**, *128*, 2017.
(104) Risko, C.; Coropceanu, V.; Barlow, S.; Geskin, V.; Schmidt, K.; Gruhn, N. E.; Marder, S. R.; Bredas, J. L. *J. Phys. Chem. C* **2008**, *112*, 7959.
(105) Wojdel, J. C.; Bromley, S. T. *J. Mol. Model.* **2005**, *11*, 288.
(106) Wojdel, J. C.; Moreira, I. P. R.; Bromley, S. T.; Illas, F. *J. Chem. Phys.* **2008**, *128*, 0447131.
(107) Londergan, C. H.; Kubiak, C. P. *Chem.—Eur. J.* **2003**, *9*, 5962.
(108) Low, P. J. *Dalton Trans.* **2005**, 2821.
(109) Yuan, P.; Liu, S. H.; Xiong, W. C.; Yin, J.; Yu, G. A.; Sung, H. Y.; Williams, I. D.; Jia, G. C. *Organometallics* **2005**, *24*, 1452.
(110) Owen, G. R.; Stahl, J.; Hampel, F.; Gladysz, J. A. *Organometallics* **2004**, *23*, 5889.
(111) Endicott, J. F.; Chen, Y. J. *Inorg. Chim. Acta* **2007**, *360*, 913.
(112) Akita, M.; Tereda, M.; Oyama, S.; Sugimoto, S.; Moro-oka, Y. *Organometallics* **1991**, *10*, 1561.
(113) Caulton, K. G.; Cayton, R. H.; Chisholm, M. H.; Huffman, J. C.; Lobkovsky, E. B.; Xue, Z. *Organometallics* **1992**, *11*, 321.
(114) Chen, M. C.; Tsai, Y. J.; Chen, C. T.; Lin, Y. C.; Tseng, T. W.; Lee, G. H.; Wang, Y. *Organometallics* **1991**, *10*, 378.
(115) Heidrich, J.; Stelmann, M.; Appel, M.; Beck, W. *Organometallics* **1990**, *9*, 1296.
(116) Belanzoni, P.; Re, N.; Sgamellotti, A.; Floriani, C. *J. Chem. Soc., Dalton Trans.* **1998**, 1825.
(117) Bruce, M. I. *Coord. Chem. Rev.* **1997**, *166*, 91.
(118) Bruce, M. I. *Chem. Rev.* **1998**, *98*, 2797.
(119) Coat, F.; Paul, F.; Lapinte, C.; Toupet, L.; Costuas, K.; Halet, J. F. *J. Organomet. Chem.* **2003**, *683*, 368.
(120) Mohr, W.; Stahl, J.; Hampel, F.; Gladysz, J. A. *Chem.—Eur. J.* **2003**, *9*, 3324.
(121) Yuan, P.; Wu, X. H.; Yu, G. A.; Du, D.; Liu, S. H. *J. Organomet. Chem.* **2007**, *692*, 3588.
(122) Fan, Q.; Pfeiffer, G. V. *Chem. Phys. Lett.* **1989**, *162*, 472.
(123) Weng, W. Q.; Bartik, T.; Brady, M.; Bartik, B.; Ramsden, J. A.; Arif, A. M.; Gladysz, J. A. *J. Am. Chem. Soc.* **1995**, *117*, 11922.
(124) Belanzoni, P.; Re, N.; Sgamellotti, A. *J. Organomet. Chem.* **2002**, *656*, 156.
(125) Xia, H. P.; Wu, W. F.; Ng, W. S.; Williams, I. D.; Jia, G. *Organometallics* **1997**, *16*, 2940.
(126) Bildstein, B.; Loza, O.; Chizhov, Y. *Organometallics* **2004**, *23*, 1825.
(127) Bruce, M. I.; Costuas, K.; Ellis, B. G.; Halet, J. F.; Low, P. J.; Moubaraki, B.; Murray, K. S.; Ouddai, N.; Perkins, G. J.; Skelton, B. W.; White, A. H. *Organometallics* **2007**, *26*, 3735.
(128) Bruce, M. I.; Ellis, B. G.; Gaudio, M.; Lapinte, C.; Melino, G.; Paul, F.; Skelton, B. W.; Smith, M. E.; Toupet, L.; White, A. H. *Dalton Trans.* **2004**, 1601.
(129) Kheradmandan, S.; Venkatesan, K.; Blacque, O.; Schmalle, H. W.; Berke, H. *Chem.—Eur. J.* **2004**, *10*, 4872.
(130) Bartlett, M. J.; Hill, A. F.; Smith, M. K. *Organometallics* **2005**, *24*, 5795.
(131) Venkatesan, K.; Fox, T.; Schmalle, H. W.; Berke, H. *Organometallics* **2005**, *24*, 2834.
(132) Dewhurst, R. D.; Hill, A. F.; Willis, A. C. *Organometallics* **2004**, *23*, 5903.
(133) Bruce, M. I.; Cole, M. L.; Gaudio, M.; Skelton, B. W.; White, A. H. *J. Organomet. Chem.* **2006**, *691*, 4601.
(134) Cowan, D. O.; Levanda, C.; Park, J.; Kaufman, F. *Acc. Chem. Res.* **1973**, *6*, 1.
(135) Levanda, C.; Bechgaard, K.; Cowan, D. O. *J. Org. Chem.* **1976**, *41*, 2700.
(136) Adams, R. D.; Qu, B.; Smith, M. D. *Organometallics* **2002**, *21*, 3867.
(137) Xu, G. L.; Xi, B.; Updegraff, J. B.; Protasiewicz, J. D.; Ren, T. *Organometallics* **2006**, *25*, 5213.
(138) Richardson, D. E.; Taube, H. *Inorg. Chem.* **1981**, *20*, 1278.
(139) de Quadras, L.; Hampel, F.; Gladysz, J. A. *Dalton Trans.* **2006**, 2929.
(140) Zheng, Q. L.; Hampel, F.; Gladysz, J. A. *Organometallics* **2004**, *23*, 5896.
(141) Zhuravlev, F.; Gladysz, J. A. *Chem.—Eur. J.* **2004**, *10*, 6510.
(142) Zheng, Q. L.; Bohling, J. C.; Peters, T. B.; Frisch, A. C.; Hampel, F.; Gladysz, J. A. *Chem.—Eur. J.* **2006**, *12*, 6486.
(143) Zheng, Q.; Gladysz, J. A. *J. Am. Chem. Soc.* **2005**, *127*, 10508.
(144) Owen, G. R.; Stahl, J.; Hampel, F.; Gladysz, J. A. *Chem.—Eur. J.* **2008**, *14*, 73.
(145) Barlow, S.; Risko, C.; Coropceanu, V.; Tucker, N. M.; Jones, S. C.; Levi, Z.; Khrustalev, V. N.; Antipin, M. Y.; Kinnibrugh, T. L.; Timofeeva, T.; Marder, S. R.; Bredas, J. L. *Chem. Commun.* **2005**, 764.
(146) Barlow, S.; Marder, S. R. *Chem. Commun.* **2000**, 1555.
(147) Rosokha, S. V.; Sun, D. L.; Kochi, J. K. *J. Phys. Chem. A* **2002**, *106*, 2283.
(148) Ribou, A. C.; Launay, J. P.; Sachtleben, M. L.; Li, H.; Spangler, C. W. *Inorg. Chem.* **1996**, *35*, 3735.
(149) Delgado-Pena, F.; Talham, D. R.; Cowan, D. O. *J. Organomet. Chem.* **1983**, *253*, C43.
(150) Bolton, S. L.; Schuehler, D. E.; Niu, X.; Gopal, L.; Sponsler, M. B. *J. Organomet. Chem.* **2006**, *691*, 5298.
(151) Grubbs, R. H. *Tetrahedron* **2004**, *60*, 7117.
(152) Schwab, P.; Grubbs, R. H.; Ziller, J. W. *J. Am. Chem. Soc.* **1996**, *118*, 100.
(153) Creutz, C.; Taube, H. *J. Am. Chem. Soc.* **1973**, *95*, 1086.
(154) Gong, L.; Wu, L. Q.; Lin, Y. M.; Zhang, H.; Yang, F. Z.; Wen, T. B.; Xia, H. P. *Dalton Trans.* **2007**, 4122.
(155) Liu, S. H.; Hu, Q. Y.; Xue, P.; Wen, T. B.; Williams, I. D.; Jia, G. C. *Organometallics* **2005**, *24*, 769.
(156) Liu, S. H.; Xia, H. P.; Wen, T. B.; Zhou, Z. Y.; Jia, G. C. *Organometallics* **2003**, *22*, 737.
(157) Liu, S. H.; Chen, Y. H.; Wan, K. L.; Wen, T. B.; Zhou, Z. Y.; Lo, M. F.; Williams, I. D.; Jia, G. C. *Organometallics* **2002**, *21*, 4984.
(158) Maurer, J.; Sarkar, B.; Kaim, W.; Winter, R. F.; Zalis, S. *Chem.—Eur. J.* **2007**, *13*, 10257.
(159) Maurer, J.; Sarkar, B.; Schwederski, B.; Kaim, W.; Winter, R. F.; Zalis, S. *Organometallics* **2006**, *25*, 3701.
(160) Maurer, J.; Winter, R. F.; Sarkar, B.; Fiedler, J.; Zalis, S. *Chem. Commun.* **2004**, 1900.
(161) Yin, J.; Yu, G. A.; Tu, H. Y.; Liu, S. H. *Appl. Organomet. Chem.* **2006**, *20*, 869.
(162) Irie, M. *Chem. Rev.* **2000**, *100*, 1683.
(163) Gagliardo, M.; Amijs, C. H. M.; Lutz, M.; Spek, A. L.; Havenith, R. W. A.; Hartl, F.; van Klink, G. P. M.; van Koten, G. *Inorg. Chem.* **2007**, *46*, 11133.
(164) Xia, J. L.; Wu, X. H.; Lu, Y. H.; Chen, G.; Jin, S.; Yu, G. A.; Liu, S. H. *Organometallics* **2009**, *28*, 2701.
(165) Aguirre-Etcheverry, P.; Ashley, A.; Green, J.; Cowley, A.; Thomson, A.; O'Hare, D. *Dalton Trans.* submitted for publication.
(166) Akita, M.; Tanaka, Y.; Naitoh, C.; Ozawa, T.; Hayashi, N.; Takeshita, M.; Inagaki, A.; Chung, M. C. *Organometallics* **2006**, *25*, 5261.
(167) Hamon, P.; Justaud, F.; Cador, O.; Hapiot, P.; Rigaut, S.; Toupet, L.; Ouahab, L.; Stueger, H.; Hamon, J. R.; Lapinte, C. *J. Am. Chem. Soc.* **2008**, *130*, 17372.
(168) Matsuura, Y.; Tanaka, Y.; Akita, M. *J. Organomet. Chem.* **2009**, *694*, 1840.
(169) Rigaut, S.; Olivier, C.; Costuas, K.; Choua, S.; Fadhel, O.; Massue, J.; Turek, P.; Saillard, J. Y.; Dixneuf, P. H.; Touchard, D. *J. Am. Chem. Soc.* **2006**, *128*, 5859.
(170) Fox, M. A.; Farmer, J. D.; Roberts, R. L.; Humphrey, M. G.; Low, P. J. *Organometallics* **2009**, *28*, 5266.
(171) Gao, L. B.; Kan, J.; Fan, Y.; Zhang, L. Y.; Liu, S. H.; Chen, Z. N. *Inorg. Chem.* **2007**, *46*, 5651.
(172) Olivier, C.; Kim, B.; Touchard, D.; Rigaut, S. *Organometallics* **2008**, *27*, 509.
(173) Field, L. D.; Magill, A. M.; Shearer, T. K.; Colbran, S. B.; Lee, S. T.; Dalgarno, S. J.; Bhadbhade, M. M. *Organometallics* **2010**, *29*, 957.
(174) Klein, A.; Lavastre, O.; Fiedler, J. *Organometallics* **2006**, *25*, 635.
(175) Medei, L.; Orian, L.; Semeikin, O. V.; Peterleitner, M. G.; Ustynyuk, N. A.; Santi, S.; Durante, C.; Ricci, A.; Lo Sterzo, C. *Eur. J. Inorg. Chem.* **2006**, 2582.
(176) Lapinte, C. *J. Organomet. Chem.* **2008**, *693*, 793.
(177) de Montigny, F.; Argouarch, G.; Costuas, K.; Halet, J. F.; Roisnel, T.; Toupet, L.; Lapinte, C. *Organometallics* **2005**, *24*, 4558.

(178) de Montigny, F.; Argouarch, G.; Roisnel, T.; Toupet, L.; Lapinte, C.; Lam, S. C. F.; Tao, C. H.; Yam, V. W. W. *Organometallics* **2008**, *27*, 1912.
(179) Justaud, F.; Argouarch, G.; Ibn Ghazala, S.; Toupet, L.; Paul, F.; Lapinte, C. *Organometallics* **2008**, *27*, 4260.
(180) Ibn Ghazala, S.; Paul, F.; Toupet, L.; Roisnel, T.; Hapiot, P.; Lapinte, C. *J. Am. Chem. Soc.* **2006**, *128*, 2463.
(181) Paul, F.; Goeb, S.; Justaud, F.; Argouarch, G.; Toupet, L.; Ziessel, R. F.; Lapinte, C. *Inorg. Chem.* **2007**, *46*, 9036.
(182) Tanaka, Y.; Shaw-Taberlet, J. A.; Justaud, F.; Cador, O.; Roisnel, T.; Akita, M.; Hamon, J. R.; Lapinte, C. *Organometallics* **2009**, *28*, 4656.
(183) Engtrakul, C.; Sita, L. R. *Organometallics* **2008**, *27*, 927.
(184) Astruc, D. *Acc. Chem. Res.* **1997**, *30*, 383.
(185) Astruc, D. *J. Organomet. Chem.* **2004**, *689*, 4332.
(186) Rausch, M. D.; Spink, W. C.; Conway, B. G.; Rogers, R. D.; Atwood, J. L. *J. Organomet. Chem.* **1990**, *383*, 227.
(187) Li, B.; Wang, B. Q.; Xu, S. S.; Zhou, X. Z.; Song, H. B. *Organometallics* **2006**, *25*, 1158.
(188) Baum, E.; Matern, E.; Pikies, J.; Robaszkiewiez, A. *Z. Anorg. Allg. Chem.* **2004**, *630*, 1090.
(189) Han, H.; Johnson, S. A. *Eur. J. Inorg. Chem.* **2008**, 471.
(190) Lee, S. G.; Lee, S. S.; Chung, Y. K. *Inorg. Chim. Acta* **1999**, *286*, 215.
(191) Santi, S.; Durante, C.; Donoli, A.; Bisello, A.; Orian, L.; Ceccon, A.; Crociani, L.; Benetollo, F. *Organometallics* **2009**, *28*, 3319.
(192) Nafady, A.; Chin, T. T.; Geiger, W. E. *Organometallics* **2006**, *25*, 1654.
(193) Chin, T. T.; Geiger, W. E.; Rheingold, A. L. *J. Am. Chem. Soc.* **1996**, *118*, 5002.
(194) Zhu, B. L.; Miljanic, O. S.; Vollhardt, K. P. C.; West, M. J. *Synthesis* **2005**, 3373.
(195) Lin, J.; Luo, S. A.; Cheng, B.; Wang, B. Q.; Xu, S. S.; Song, H. B. *Appl. Organomet. Chem.* **2006**, *20*, 375.
(196) Zhang, Q. F.; Cheung, K. M.; Williams, I. D.; Leung, W. H. *Eur. J. Inorg. Chem.* **2005**, 4780.
(197) Green, M. L. H.; Lowe, N. D.; O'Hare, D. *J. Chem. Soc., Chem. Commun.* **1986**, 1547.
(198) Cabeza, J. A.; del Rio, I.; Fernandez-Colinas, J. M.; Garcia-Alvarez, P.; Miguel, D. *Organometallics* **2007**, *26*, 1414.
(199) Tan, Y. L. K.; Leong, W. K. *J. Organomet. Chem.* **2007**, *692*, 768.
(200) Ascenso, J. R.; Dias, A. R.; Duarte, M. T.; Gomes, P. T.; Marote, J. N.; Ribeiro, A. F. G. *J. Organomet. Chem.* **2001**, *632*, 164.
(201) Kerber, R. C.; Waldbaum, B. R. *J. Organomet. Chem.* **1996**, *513*, 277.
(202) Khayatpoor, R.; Shapley, J. R. *Organometallics* **2000**, *19*, 2382.
(203) Wang, B. Q.; Xu, S. S.; Zhou, X. T. *J. Organomet. Chem.* **1997**, *540*, 101.
(204) Xie, W.; Wang, B.; Xu, S.; Zhou, X. *Polyhedron* **1999**, *18*, 1647.
(205) Chen, D. F.; Mu, B.; Xu, S. S.; Wang, B. Q. *J. Organomet. Chem.* **2006**, *691*, 3823.
(206) Mutseneck, E. V.; Petrovskii, P. K.; Kudinov, A. R. *Russ. Chem. Bull.* **2004**, *53*, 2090.
(207) Mutseneck, E. V.; Starikova, Z. A.; Lyssenko, K. A.; Petrovskii, P. V.; Zanello, P.; Corsini, M.; Kudinov, A. R. *Eur. J. Inorg. Chem.* **2006**, 4519.
(208) Kukharenko, S. V.; Strelets, V. V.; Kudinov, A. R.; Kreidlin, A. Z.; Peterleitner, M. G.; Denisovich, L. I.; Rybinskaya, M. I. *J. Organomet. Chem.* **1996**, *519*, 1.
(209) Gassman, P. G.; Winter, C. H. *J. Am. Chem. Soc.* **1988**, *110*, 6130.
(210) Gusev, O. V.; Ievlev, M. A.; Peterleitner, M. G.; Peregudova, S. M.; Denisovich, L. I.; Petrovskii, P. V.; Ustynyuk, N. A. *J. Organomet. Chem.* **1997**, *534*, 57.
(211) Chen, D. F.; Xu, S. S.; Song, H. B.; Wang, B. Q. *Eur. J. Inorg. Chem.* **2008**, 1854.
(212) Ashley, A. E., PhD Thesis, University of Oxford, Oxford, U.K., 2005.
(213) Summerscales, O. T.; Cloke, F. G. N. *Coord. Chem. Rev.* **2006**, *250*, 1122.
(214) Jones, S. C.; Roussel, P.; Hascall, T.; O'Hare, D. *Organometallics* **2006**, *25*, 221.
(215) Balazs, G.; Cloke, F. G. N.; Harrison, A.; Hitchcock, P. B.; Green, J.; Summerscales, O. T. *Chem. Commun.* **2007**, 873.
(216) Balazs, G.; Cloke, F. G. N.; Gagliardi, L.; Green, J. C.; Harrison, A.; Hitchcock, P. B.; Shahi, A. R. M.; Summerscales, O. T. *Organometallics* **2008**, *27*, 2013.
(217) Ashley, A. E.; Cowley, A. R.; O'Hare, D. *Eur. J. Org. Chem.* **2007**, 2239.
(218) Ashley, A. E.; Cowley, A. R.; O'Hare, D. *Chem. Commun.* **2007**, 1512.
(219) Ashley, A. E.; Cooper, R. T.; Wildgoose, G. G.; Green, J. C.; O'Hare, D. *J. Am. Chem. Soc.* **2008**, *130*, 15662.
(220) Cooper, R. T. Part Two Thesis, University of Oxford, Oxford, U.K., 2007.
(221) Ashley, A. E.; Balazs, G.; Cowley, A. R.; Green, J. C.; O'Hare, D. *Organometallics* **2007**, *26*, 5517.
(222) Reingold, J. A.; Virkaitis, K. L.; Carpenter, G. B.; Sun, S. H.; Sweigart, D. A.; Czech, P. T.; Overly, K. R. *J. Am. Chem. Soc.* **2005**, *127*, 11146.
(223) Orian, L.; Ganis, P.; Santi, S.; Ceccon, A. *J. Organomet. Chem.* **2005**, *690*, 482.
(224) Alt, H. G.; Samuel, E. *Chem. Soc. Rev.* **1998**, *27*, 323.
(225) Kirillov, E.; Saillard, J. Y.; Carpentier, J. F. *Coord. Chem. Rev.* **2005**, *249*, 1221.
(226) Bochmann, M.; Lancaster, S. J.; Hursthouse, M. B.; Mazid, M. *Organometallics* **1993**, *12*, 4718.
(227) Decken, A.; MacKay, A. J.; Brown, M. J.; Bottomley, F. *Organometallics* **2002**, *21*, 2006.
(228) Moss, J. E. PhD Thesis, University of Oxford, Oxford, U.K., 2007.
(229) Moss, J. E.; Thomas, J.; Ashley, A. E.; Cowley, A. R.; O'Hare, D. *Organometallics* **2006**, *25*, 4279.
(230) Morrison, W. H.; Ho, E. Y.; Hendrickson, D. N. *Inorg. Chem.* **1975**, *14*, 500.
(231) Stahl, J.; Mohr, W.; de Quadras, L.; Peters, T. B.; Bohling, J. C.; Martin-Alvarez, J. M.; Owen, G. R.; Hampel, F.; Gladysz, J. A. *J. Am. Chem. Soc.* **2007**, *129*, 8282.
(232) Aguirre-Etcheverry, P. L. PhD Thesis, University of Oxford, Oxford, U.K., 2008.

CR9003852